chemosensors

MDPI

Review

Non-Enzymatic Electrochemical Glucose Sensors Based on Metal Oxides and Sulfides: Recent Progress and Perspectives

Haibing Zhu, Feng Shi, Maoying Peng, Ye Zhang, Sitian Long, Ruixin Liu, Juan Li * and Zhanjun Yang *

School of Chemistry and Chemical Engineering, Yangzhou University, Yangzhou 225002, China; z18716784607@163.com (H.Z.); m18805274649@163.com (F.S.); pmy15860902493@163.com (M.P.); 13142553167@163.com (Y.Z.); 15062852573@163.com (S.L.); ruixinl_h@163.com (R.L.)
* Correspondence: lijuan@yzu.edu.cn (J.L.); zjyang@yzu.edu.cn (Z.Y.); Tel.: +86-514-8797-2034 (J.L.); +86-514-8797-2034 (Z.Y.)

Abstract: With the sudden advancement of glucose biosensors for monitoring blood glucose levels for the prevention and diagnosis of diabetes, non-enzymatic glucose sensors have aroused great interest owing to their sensitivity, stability, and economy. Recently, researchers have dedicated themselves to developing non-enzymatic electrochemical glucose sensors for the rapid, convenient, and sensitive determination of glucose. However, it is desirable to explore economic and effective nanomaterials with a high non-enzymatic catalysis performance toward glucose to modify electrodes. Metal oxides (MOs) and metal sulfides (MSs) have attracted extensive interest among scholars owing to their excellent catalytic activity, good biocompatibility, low cost, simple synthesis process, and controllable morphology and structure. Nonetheless, the exploitation of MOs and MSs in non-enzymatic electrochemical glucose sensors still suffers from relatively low conductivity and biocompatibility. Therefore, it is of significance to integrate MOs and MSs with metal/carbon/conducive polymers to modify electrodes for compensating the aforementioned deficiency. This review introduces the recent developments in non-enzymatic electrochemical glucose sensors based on MOs and MSs, focusing on their preparation methods and how their structural composition influences sensing performance. Finally, this review discusses the prospects and challenges of non-enzymatic electrochemical glucose sensors.

Keywords: metal oxides; metal sulfides; glucose; non-enzymatic; electrochemical sensor

Received: 30 November 2024
Revised: 6 January 2025
Accepted: 9 January 2025
Published: 16 January 2025

Citation: Zhu, H.; Shi, F.; Peng, M.; Zhang, Y.; Long, S.; Liu, R.; Li, J.; Yang, Z. Non-Enzymatic Electrochemical Glucose Sensors Based on Metal Oxides and Sulfides: Recent Progress and Perspectives. *Chemosensors* **2025**, *13*, 19. https://doi.org/10.3390/chemosensors13010019

1. Introduction

Diabetes, as a chronic systemic metabolic disorder, arises from either insufficient insulin secretion or an insufficient utilization of insulin in the human body, resulting in elevated blood glucose levels [1,2]. Diabetes may lead to a variety of complications, including unintended weight loss, renal failure, cardiovascular disease (CVD), retinopathy, and stroke, which can even lead to death [3–5]. According to the International Diabetes Federation (IDF), the global diabetic patient population is steadily rising, with diabetes projected to emerge as the seventh most-prominent cause of mortality worldwide by 2040 [6]. Consequently, continuous blood sugar monitoring of patients plays a pivotal role in early diabetes prevention and diagnosis.

To date, various methods have been developed for serum glucose detection, such as enzyme electrodes [7], the hexokinase (HK) method [8], spectrophotometry [9], high-performance liquid chromatography (HPLC) [10], and urine glucose test strips. In laboratories, widely studied methods for glucose detection include colorimetry [11], electrochemistry [12], chemiluminescence [13], surface plasmon resonance (SPR) [14], and

fluorescence [15]. Clinically, enzyme-based electrochemical sensors are the mainstream glucose detection method and have undergone three iterations of updates. First-generation glucose oxidase (GOx)-based sensors rely on oxygen and are susceptible to interference from electroactive substances, such as acetaminophen, ascorbic acid, and uric acid. Second-generation glucose sensors facilitate electron transfer from the redox center of GOx to the electrode surface by introducing redox mediators, but they may face issues, such as toxicity and stability problems, due to the leaching of these mediators. Third-generation glucose sensors focus on achieving direct electron transfer (DET) between GOx and the electrode without the need for redox mediators. However, third-generation glucose sensors are still in the research stage [16]. Although enzyme-based sensors currently dominate the glucose sensor market, natural enzymes may be affected by environmental factors, such as pH, humidity, and temperature. Non-enzymatic electrochemical glucose sensors are expected to rely on the direct redox reactions of glucose on electrode materials, thus avoiding the use of biological enzymes, which has been a goal that researchers have been striving to achieve [17].

Non-enzymatic glucose sensors employing precious-metal electrode materials, like platinum, gold, palladium, and silver, have demonstrated remarkable benefits regarding sensitivity, selectivity, and response time [18,19]. Nevertheless, the utilization of precious metals faces constraints due to their low reserves and high costs, making it difficult to achieve large-scale application. The rapid advancement of nanomaterials has generated a growing fascination with the utilization of metals [20], alloys [21], metal oxides (MOs) [22,23], metal sulfides (MSs) [24,25], carbon materials [26], and their composites as electrocatalysts for emerging non-enzymatic electrochemical glucose sensors. Recently, researchers have been committed to developing non-enzymatic electrochemical glucose sensors based on MOs and MSs due to their excellent catalytic activity, good biocompatibility, cost-effectiveness, simple synthesis process, and controllable morphology and structure. MOs, known for their diverse oxidation states, exhibit substantial promise as excellent candidate materials for non-enzymatic electrochemical glucose sensors, primarily owing to their low preparation cost, outstanding catalytic activity, and inherent stability [27–29]. Moreover, non-enzymatic electrochemical glucose sensors with a high catalytic performance can be effectively created by fabricating metal oxides with large specific surface areas and multi-component composites providing more catalytic active sites. Recently, MOs, such as iron (Fe)-based [30], cobalt (Co)-based [31,32], copper (Cu)-based [33], nickel (Ni)-based [34–36], zinc (Zn)-based [37], titanium (Ti)-based [38], and their composites, have found extensive application as catalysts in non-enzymatic electrochemical glucose sensors. Compared with the corresponding MOs, MSs exhibit a smaller band gap, superior conductivity, and better stability. Furthermore, MSs can be synthesized via a simple fabrication procedure without the high-temperature annealing process. Similar to MOs, some MSs, such as NiS, Ni_3S_2, CoS, and Co_3S_4, exist in various chemical states, showing proficient glucose oxidation capabilities. Recently, MSs based on copper (Cu) [39], molybdenum (Mo) [40], cobalt (Co) [41], and nickel (Ni) [42] have demonstrated notable stability and noteworthy catalytic activity, and have been increasingly studied in non-enzymatic electrochemical glucose sensors. Interestingly, researchers are dedicated to developing novel non-enzymatic electrochemical glucose sensors based on MOs or MSs by enhancing the conductivity, increasing the specific surface area, and constructing heterojunctions. However, the inherent conductivity of MOs or MSs is relatively poor. Consequently, a common strategy is to combine them with conductive materials, such as carbon-based materials or conductive polymers, including reduced graphene oxide (rGO), carbon nanotubes (CNTs), carbon nanofibers (CNFs), polypyrrole (PPy), polyaniline (PANI), and poly(3,4-ethylenedioxythiophene) (PEDOT). In addition, MOs or MSs of different types of metals

can be combined to construct heterojunctions, which can not only improve the conductivity of the electrode material, but also enhance the catalytic activity through synergistic effects.

As the awareness of diabetes increases, the interest of researchers in this field will continue to increase. In recent years, scientists have conducted extensive research and experiments on the application of electrochemical sensors for glucose detection (Figure 1a). In this review, we focus on the latest progress in the field of non-enzymatic electrochemical glucose sensors based on MOs and MSs (Figure 1b). This paper summarizes the preparation methods, structural characteristics, morphologies, and corresponding sensing properties of various MOs and MSs. In addition, we analyze the reasons for the synergistic enhancement of multi-component electrode materials in comparison to their single components. Finally, we also proposed the issues and challenges faced by non-enzymatic electrochemical glucose sensors based on MOs and MSs, and presented a certain prospect for the future development of non-enzymatic electrochemical glucose sensors.

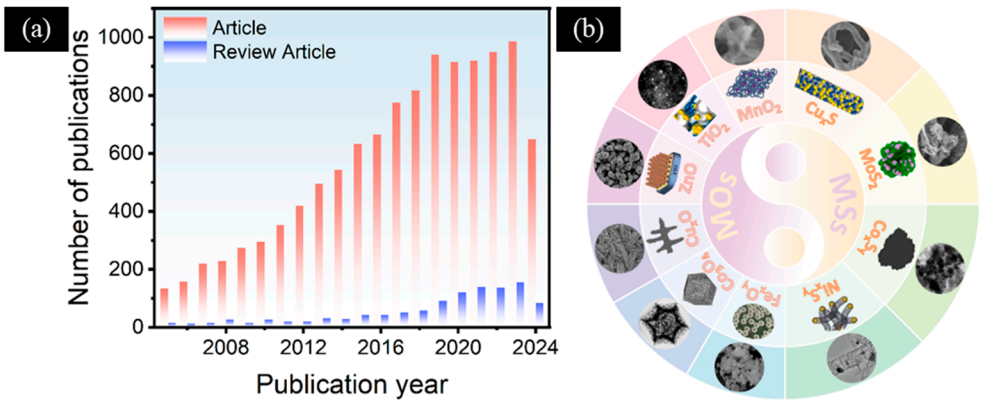

Figure 1. (**a**) Statistics of the number of recent publications regarding electrochemical glucose sensors versus the year of publication (data collected from the ISI Web of Science database using "electrochemical", "glucose", and "sensor" as search terms on 10 October 2024). (**b**) MOs and MSs for the modification of electrodes in non-enzymatic electrochemical glucose sensors. Fe_xO_y: Reproduced with permission [43]. Copyright 2024, Elsevier, 2024. Co_xO_y: Reproduced with permission [44]. Copyright 2022, Elsevier. Cu_xO: Reproduced with permission [33]. Copyright 2021, ScienceDirect. ZnO: Reproduced with permission [45]. Copyright 2021, Elsevier. TiO_2: Reproduced with permission [46]. MnO_2: Copyright 2020, Elsevier. Reproduced with permission [47]. Copyright 2023, Elsevier. Cu_xS: Reproduced with permission [48]. Copyright 2024, Elsevier. MoS_2: Reproduced with permission [49]. Copyright 2024, Elsevier. Co_xS_y: Reproduced with permission [50]. Copyright 2023, Elsevier. Ni_xS_y: Reproduced with permission [51]. Copyright 2022, Elsevier.

2. MO-Based Non-Enzymatic Electrochemical Glucose Sensors

2.1. Iron-Based Oxides

Since Godarzi et al. [52] originally reported Fe_3O_4/functionalized-MWCNTs/glassy carbon electrode (GCE)-based non-enzymatic electrochemical sensors in 2014, Fe_3O_4 NPs have emerged as an outstanding catalyst for innovative sensing platforms due to their oxidation stability, excellent catalytic properties, and biocompatibility [53–55]. Moreover, hematite (Fe_2O_3), another typical iron-based oxide, exhibits outstanding electrical conductivity, has a low cost, good chemical stability, and high catalytic activity [56]. For example, Luo et al. [57] reported that the NiO/Fe_2O_3-based non-enzymatic glucose sensor achieved sensitive glucose detection in a 0.05 M PBS (pH = 7.0) solution. Therefore, both of them and their composites possess the advantages of a wide linear range, high sensitivity, and great anti-interference ability in the application of electrochemical glucose sensors.

To address the relatively low catalytic activity caused by the traditional agglomeration of iron-based oxides, various improved strategies have been studied to enhance their

catalysis performance for establishing glucose biosensors with superior properties. For instance, combining conductive polymers, carbon materials, and metal–organic frameworks (MOFs) can significantly improve the analytical performance of glucose sensors. Ghaffarirad et al. [43] reported a non-enzymatic electrochemical sensor using PANI and Fe_3O_4@MIL-101-NH_2-modified nitrogen-doped functionalized graphene (NFG), shown in Figure 2a. Using mercaptoacetic acid-functionalized magnetic Fe_3O_4 nanoparticles as the core, the Fe_3O_4@MIL-101-NH_2 core–shell structure was synthesized through the in situ growth of MOFs. Then, the authors combined MOFs with PANI and NFG to enhance the conductivity, stability, and sensitivity, which compensates for the limits of MOFs. This work shows that we can optimize the performance by regulating the composition, morphology, and structure of materials. Typically, oxides obtained by the controlled pyrolysis of MOFs can expose highly active metal sites. For instance, Abrori et al. [58] reported FeBDC-derived Fe_3O_4 for a non-enzymatic electrochemical glucose sensor. Compared with FeBDC, FeBDC-derived Fe_3O_4 was broken into small particles due to the pyrolysis of organic ligands. More interestingly, Liu et al. [59] reported melamine and Prussian blue (PB)-derived g-C_3N_4/α-Fe_2O_3 composites for a sensitive non-enzymatic electrochemical glucose sensor. Specifically, PB was obtained by co-precipitating a mixed solution of $K_3[Fe(CN)_6]$ and $FeCl_3$ at an ambient temperature, then PB and HCl were added to absolute ethanol containing melamine and stirred, followed by the evaporation of the solvent. Finally, the obtained product was annealed for 4 h at 550 °C to prepare g-C_3N_4/α-Fe_2O_3 (Figure 2b). The g-C_3N_4/α-Fe_2O_3/GCE electrode exhibited a higher current response in the KOH solution compared to the other electrodes (Figure 2c) and the sensor possessed a wide linear range from 2 µM to 2.4 mM (Figure 2d). This can be ascribed to two reasons: (i) the two-dimensional (2D)-layered structure of g-C_3N_4 provided a large specific surface area for anchoring and dispersing α-Fe_2O_3 nanoparticles; (ii) glucose molecules were preferentially adsorbed to the electrode surface by the abundant N on the surface of g-C_3N_4, which was followed by electrochemical oxidation under the synergistic effect of g-C_3N_4 and α-Fe_2O_3.

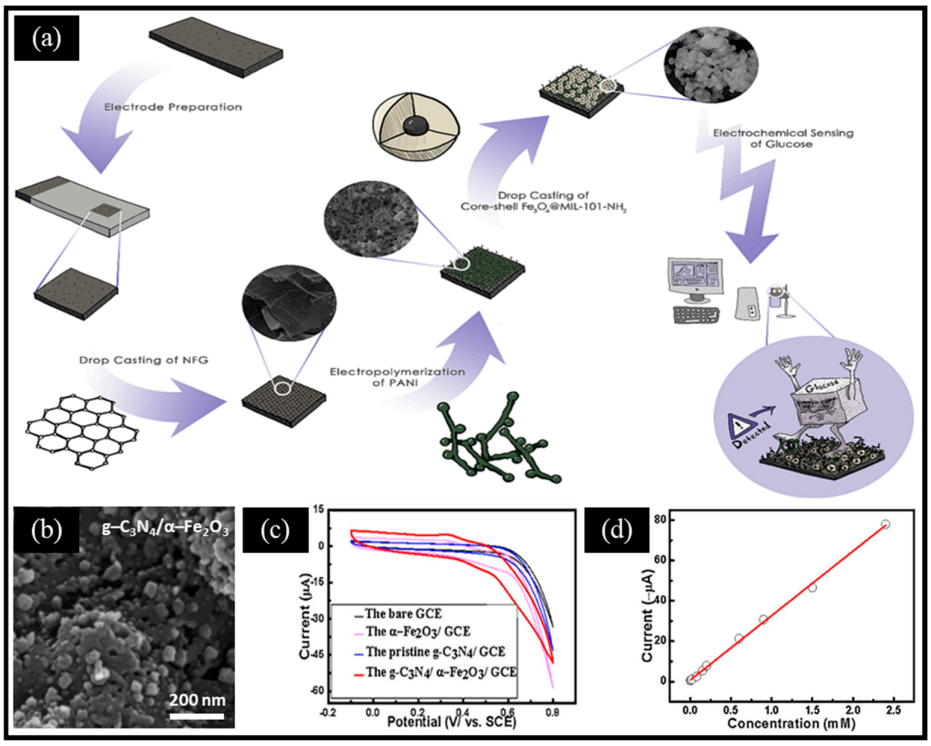

Figure 2. (**a**) Schematic diagram of the biosensing platform based on the GS/NFG/PANI/Fe_3O_4@MIL-101-NH_2 electrode. (**b**) SEM image of g-C_3N_4/α-Fe_2O_3. (**c**) CV curves of glucose on the GCE, g-C_3N_4/

GCE, α-Fe_2O_3/GCE, and g-C_3N_4/α-Fe_2O_3/GCE in the 0.05 M KOH solution. (**d**) Calibration curve of the response current versus glucose concentrations. (**a**) Reproduced with permission [43]. Copyright 2024, Elsevier. (**b**–**d**) Reproduced with permission [59]. Copyright 2016, Elsevier.

2.2. Cobalt-Based Oxides

Co_3O_4 harbors cobalt ions in both divalent and trivalent states, which are crucial for the electrochemical redox process, and have been used widely. Simultaneously, the empirical evidence substantiates the role of Co_3O_4 as an effective catalyst in the domain of non-enzymatic electrochemical glucose sensors, owing to its tunable morphology, straightforward production, remarkable biocompatibility, and excellent catalytic performance [60–62]. Scholars have endeavored to design Co_3O_4 nanostructures with a variety of morphologies, including nanofibers [63,64], nanoparticles [65,66], nanosheets [67,68], and other configurations.

Taking advantage of the Co (III)/Co (IV) redox pair in Co_3O_4 that can directly achieve the electrocatalytic oxidation of glucose, more and more researchers have integrated Co_3O_4 with other nanomaterials, such as carbon-based nanomaterials, to construct highly sensitive non-enzymatic electrochemical glucose sensors. Maghsoudi et al. [69] reported a glucose biosensing platform based on an rGO/Co_3O_4/Nafion/GCE electrode. rGO/Co_3O_4 was obtained from a hydrothermal reaction of a mixed solution of cobalt chloride hexahydrate, urea, and rGO, followed by annealing the product. The electrochemical glucose sensor is evaluated via cyclic voltammetry and exhibits a linear range from 25 nM to 2.0 μM and a limit of detection (LOD) of 3.66 nM benefiting from the synergistic interplay of rGO and Co_3O_4. Meanwhile, the sensor showcased remarkable accuracy in the quantification of glucose in real samples of serum and urine. In addition, Ramesh et al. [70] developed an ultrasonic-assisted thermal reduction method for the fabrication of Co_3O_4/PPy@N-MWCNT composites. The product derived from the mixture of PPy, MWCNT, and cobalt nitrate within a hydrothermal reaction environment underwent a subsequent high-temperature annealing procedure, which achieved the conversion of $Co(OH)_2$ into Co_3O_4. The findings reveal that the dimensions of Co_3O_4 nanoparticles loaded on the N-MWCNT/PPy composite span a range of 10–20 nm (Figure 3a–d). In light of the excellent property of Co_3O_4 and its synergistic effect, Co_3O_4@N-MWCNT/PPy possesses an exceptional electrochemical performance. On the one hand, the Co_3O_4@N-MWCNT/PPy-based supercapacitor maintained an impressive 96.8% of its initial capacitance, even after undergoing 10,000 cycles. On the other hand, the authors utilized the synthesized Co_3O_4@N-MWCNT/PPy to modify GCE for constructing a electrochemical glucose sensor that exhibited a high sensitivity of 195.72 μA mM^{-1} cm^{-2} (Figure 3e). Interestingly, besides the direct utilization of carbon-based materials, MOF-derived carbon materials have also been employed to enhance the conductivity of Co_3O_4. Ouyang et al. [44] prepared rhombohedral dodecahedral ZIF-67 as the precursor that was first reduced thermally at a high temperature and then oxidized at a low temperature to yield a nitrogen-doped, hollow, carbon, porous nano-polyhedron (NHCN-Co_3O_4) (Figure 3f). The reduced cobalt species (with an average size of 40 nm, Figure 3g) located inside the carbon framework during pyrolysis acted as the catalyst to induce the growth of carbon nanotubes on the outer surface of the NHCN-Co_3O_4 framework. The NHCN-Co_3O_4/GCE electrode-based sensor manifested a wide linear range from 1.0 μM to 32.0 mM, with a low LOD of 0.2 μM. Moreover, the sensor exhibited a superior anti-interference ability and long-term stability (Figure 3h). The reasons that result in these superior performances can be summarized from two perspectives. From one perspective, carbon nanotubes derived from organic ligands enhance the electrical conductivity of the composites. From another perspective, the hollow, carbon nano-polyhedron retained the high porosity and large specific surface

area of ZIF, thereby shortening the path of electron transport and also providing more active sites for glucose oxidation.

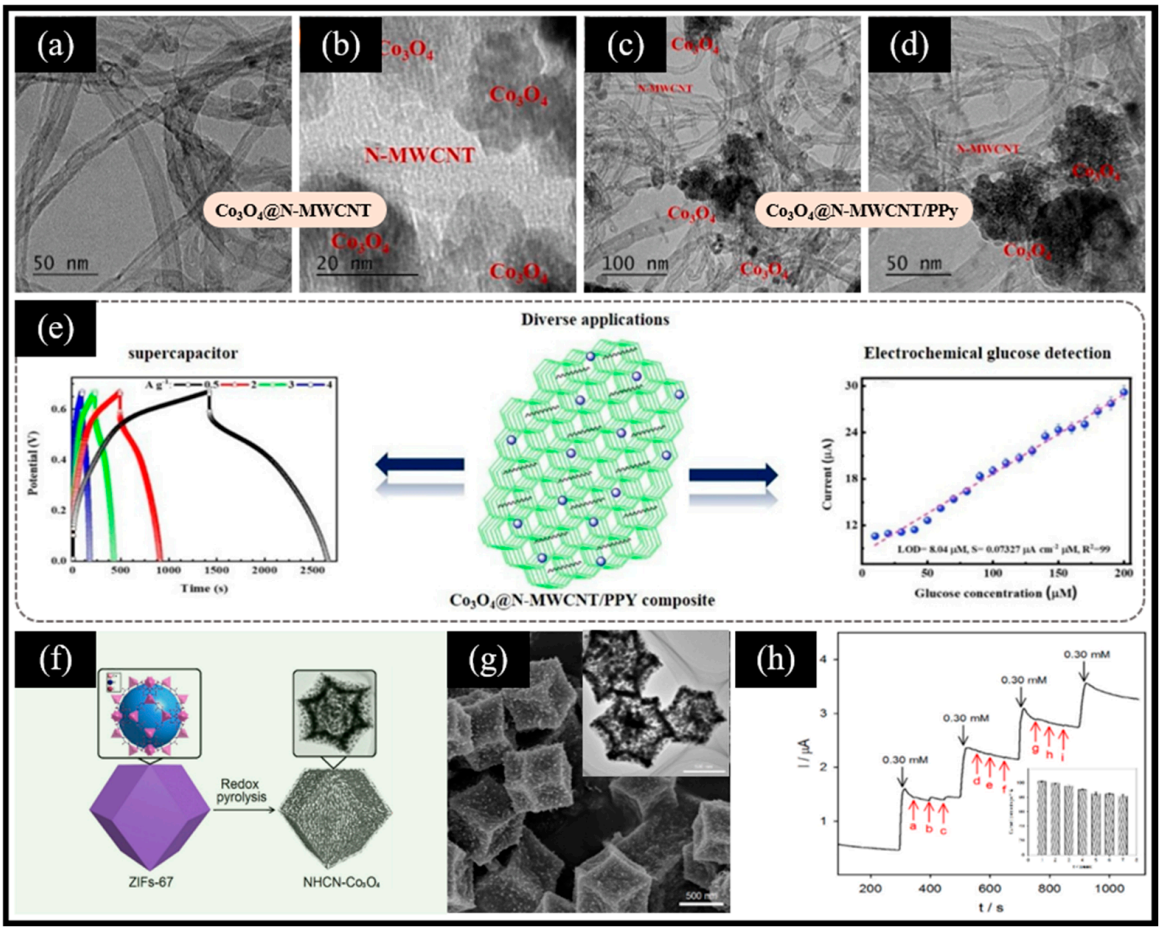

Figure 3. TEM images of the (**a**,**b**) Co_3O_4-doped N-MWCNT composites and (**c**,**d**) Co_3O_4@N-MWCNT/PPy composites. (**e**) Galvanostatic charge–discharge curve of the supercapacitor based on Co_3O_4@N-MWCNT/PPy composites (left) and calibration curve for the glucose sensor based on Co_3O_4@N-MWCNT/PPy/GCE electrodes, showing the response current in relation to glucose concentrations (right). (**f**) Illustration of the synthesis process of NHCN-Co_3O_4. (**g**) SEM image of NHCN-Co_3O_4 (inset: corresponding TEM image). (**h**) Amperometric response showing anti-interference measurements of the NHCN-Co_3O_4/GCE electrode with 0.30 mM of glucose and 0.30 mM of each possible interfering species (UA, AA, DA, leucine, glutamic acid, alanine, pyruvic acid, lactic acid, and KCl) (inset: corresponding long-term stability tests). (**a**–**e**) Reproduced with permission [70]. Copyright 2021, Elsevier. (**f**–**h**) Reproduced with permission [44]. Copyright 2022, Elsevier.

2.3. Copper-Based Oxides

Copper oxide (CuO) has been widely used in the field of electrochemical glucose sensors owing to its good stability, low cost, environmental friendliness, and straightforward synthesis methodology [71–74]. Additionally, the synergistic effect between cuprous oxide (Cu_2O) and CuO can significantly enhance electrochemical performance [75,76]. In addition to traditional chemical precipitation, hydrothermal reactions, electrospinning, and microwave-assisted techniques, some novel methods have been employed for the synthesis of copper oxide. These include dielectric barrier discharge (DBD) micro-plasma [77], vacuum spray [78], and successive ion-layer adsorption and reaction (SILAR) [79]. For example, Xiang et al. [80] obtained CuS/Cu_2O/CuO/Cu arrays on Cu foils with SILAR technology and used them directly as glucose-sensing electrodes. For glucose detection in alkaline solutions, the sensor demonstrated good selectivity, reproducibility, and stability.

Gopal et al. [81] reported a ternary composite composed of cuprous oxide and MXene embedded in porous activated carbon ($Cu_2O/M/AC$) utilizing the co-precipitation method, and its schematic diagram. Palmyra palm flowers were utilized to fabricate MXene-loaded porous activated carbon (AC) via pyrolysis and purification, in which AC and MXene were combined at a mass ratio of 1:2, and the resulting mixture underwent ultrasonic treatment to yield MXene-AC (M-AC). Ultimately, employing $Cu(CH_3COO)_2 \cdot H_2O$ as the copper source, an aqueous solution comprising $Cu(CH_3COO)_2 \cdot H_2O$, M-AC, and glucose was subjected to reflux at 90 °C to synthesize $Cu_2O/M/AC$. In comparison with M-AC and AC-Cu_2O, the $Cu_2O/M/AC$ composite demonstrated superior catalytic activity. This enhancement was attributed to the loading of Cu_2O, enhancing the active sites of the glucose sensor. Moreover, the interaction between MXene and Cu_2O facilitated electron transfer between the electrode and the electrolyte, thereby benefiting the redox reaction. It is worthy to note that the morphology of copper oxide significantly impacts the performance of electrochemical glucose sensors. For instance, Fan et al. [82] synthesized three distinct types of CuO through varying reaction conditions. When Cu^{2+} and Na_2CO_3 coexisted, Cu^{2+} was precipitated by CO_3^{2-} to form $Cu_2(OH)_2CO_3$ that was then calcined at a high temperature to obtain CuO particles with an average size of 27 nm (CuO-s). Furthermore, when the pH of the abovementioned mixture was adjusted to within 10 to 11 using NaOH and maintained at a lower temperature, platelet-shaped CuO (CuO-p) was obtained. Then, when CTAB (surfactant) and H_2O_2 were added to the solution, the following precipitation reaction occurred between Cu^{2+} and the added NaOH to obtain needle-like CuO (CuO-n). The mechanism of CuO-catalyzed glucose oxidation is shown in Equations (1) and (2):

$$CuO + OH^- \rightarrow CuOOH + e^- \quad (1)$$

$$2CuOOH + C_6H_{12}O_6\ (\text{glucose}) \rightarrow 2CuO + C_6H_{10}O_6\ (\text{gluconolactone}) + 2H_2O \quad (2)$$

On the one hand, H_2O_2 might promote CuO nucleation and growth by supplying a small quantity of oxygen vacancies during the formation of CuO and by consuming intermediate $Cu(OH)_2$, thereby causing the transformation of CuO from platelet-like (without the addition of H_2O_2) to needle-like. On the other hand, the surfactant CTAB was effective in preventing the product from agglomerating and obtaining finer needle-shaped CuO. The pre-synthesized CuO nanoparticles with different morphologies were exploited to establish non-enzymatic electrochemical glucose sensor for monitoring glucose. Interestingly, CuO-n exhibited the highest sensitivity (2.05 mA mM^{-1} cm^{-2}) compared to CuO-p (2.02 mA mM^{-1} cm^{-2}) and CuO-s@500 (1.52 mA mM^{-1} cm^{-2}), which was attributed to the excellent long-term stability of needle-like CuO as well as the high charge transfer rate. In addition to regulating the morphologies of CuO, integrating it with other nanomaterials can also enhance the properties of non-enzymatic electrochemical glucose sensors based on copper-based oxides. For instance, Zohaa et al. [83] reported a composite material loaded with copper oxide nanoparticles on mobile crystalline material-41 (Cu_2O@MCM-41), for constructing non-enzymatic electrochemical glucose sensors. First of all, Cu_2O nanoparticles with sizes ranging from 14 to 100 nm were prepared by the coprecipitation method and subsequent annealing using copper nitrate, polyvinylpyrrolidone, and sodium hydroxide as precursors. Then, Cu_2O@MCM-41 was obtained through the hydrothermal method and high-temperature calcination. Specifically, Cu_2O was dispersed on MCM-41 that can efficiently inhibit the aggregation of Cu_2O nanoparticles. The adsorption capacity of MCM-41 was enhanced by the homogeneous mesoporous structure, which offered a sizable specific surface area. CuO loading further enhanced the specific surface area and catalytic activity of CuO@MCM-41. Due to their excellent catalytic activity and biocompatibility, Au nanoparticles (Au NPs) are widely used in electrochemical glucose sensors.

Nevertheless, Au NPs may suffer from agglomeration issues, leading to a reduction in the active surface area. Thus, it is necessary to enhance the dispersibility of Au NPs to improve the performance of the sensors. By heating the mixture containing Au NPs, graphene quantum dots (GQDs), and Cu_2O, Nguyen et al. [84] designed Au/Cu_2O/GQD composites and applied them for the detection of glucose. Cu_2O, Au NP, and Au/Cu_2O/GQD possess average sizes of 30.5 nm, 29.8 nm, and 33.3 nm, respectively. The introduction of Cu_2O prevented the aggregation of Au NPs. Additionally, GQDs further improved conductivity and biocompatibility.

2.4. Zinc-Based Oxides

Zinc oxide (ZnO), an n-type II-IV semiconductor, boasts remarkable catalytic activity, controlled morphology, and excellent chemical stability [85]. Its versatile utility is evident across a multitude of applications, encompassing colorimetry [86], electrochemistry [87], photoluminescence [88], electrochemiluminescence [89], and fluorescence [90]. Due to the unique properties of ZnO, researchers have applied it to non-enzymatic electrochemical glucose sensors. For example, Ali et al. [91] reported that a vitamin B12-modified ZnO-based non-enzymatic electrochemical sensor achieved sensitive glucose detection in the range of 0.1 to 10 mM, with an LOD of 5 μM. Surprisingly, this sensor demonstrated excellent potential for glucose detection in human whole blood, with an RSD of less than 1%. Although the ZnO nanomaterial-based electrochemical glucose sensor demonstrates pronounced sensitivity, exceptional selectivity, a low LOD, and favorable biocompatibility [92], single ZnO is no longer sufficient to meet contemporary demands. Therefore, the development of ZnO-based composite materials has aroused great research interest from scholars in various fields. As an illustration, Hussein et al. [93] reported a glucose-sensing platform utilizing ZnO/Co_3O_4/rGO/GCE. The experimental results demonstrate that ZnO/Co_3O_4/rGO/GCE exhibits superior electrochemical oxidation behavior and lower charge transfer resistance (Rct) compared to ZnO/Co_3O_4/GCE, ZnO/GCE, and Co_3O_4/GCE.

Sharma et al. [94] reported a composite material in which ZnO nanorods were decorated with carbon nano-onions, referred to as ZnO/CNO. Initially, peanut-shaped ZnO nanorods 0.2–0.4 μm in length were obtained using a solvothermal reaction at 90 °C, followed by annealing at 500 °C. Subsequently, the pyrolysis product of flaxseed oil was annealed at 500 °C for 2 h to yield CNO. Finally, equal masses of ZnO and CNO were mixed to obtain ZnO/CNO. CNO was composed of graphitic carbon and diamond-like carbon, which exhibited a similarity to a spherical fullerene structure, featuring a closed carbon shell. It displayed an onion-like structure, formed by the successive wrapping of concentric fullerenes. The ZnO/CNO/GCE-based sensor, benefiting from the synergistic effects of Zn active centers and carbon materials, demonstrated notable glucose oxidation activity in the range of 0.1 mM–15 mM with a sensitivity of 606.64 μA mM^{-1} cm^{-2}. Additionally, the sensor showed an exceptional anti-interference performance along with good long-term cycle stability. Furthermore, Au NPs have been introduced to prepare compositional catalytic agents due to their intrinsic non-enzymatic catalytic performance for catalyzing the oxidation of glucose. For instance, Awais et al. [45] presented vertically aligned ZnO nanorods decorated with Au NPs (Au-ZnO NRs) and demonstrated their utilization in electrochemical glucose sensors (Figure 4a). Initially, the fluorine-doped tin oxide (FTO) electrode's surface underwent successive infiltrations with a zinc acetate solution, followed by the transformation of the zinc acetate into uniformly deposited ZnO seeds through a hydrothermal reaction. ZnO NRs (Figure 4b) were obtained by placing the electrode in a mixed solution of zinc nitrate and hexamethylenetetramine for a hydrothermal reaction. Subsequently, methanol was employed as a reducing agent to facilitate the in situ growth of

Au NPs on the surface of ZnO nanorods (Figure 4c). The sensor demonstrated a remarkable electrochemical glucose oxidation performance and showed exceptional characteristics in terms of stability, repeatability, selectivity, and its anti-interference ability. This could be attributed to two primary factors: Firstly, the presence of Au NPs significantly augmented the specific surface area, creating more active sites and promoting the electron transfer rate. Secondly, a synergistic effect between ZnO and Au further contributed to this enhancement. However, the loading of Au NPs typically requires a reduction in chloroauric acid using reducing agents under specific reaction conditions. Consequently, there is an urgent need to develop a simple and efficient technology for the deposition of Au NPs. Recently, Young et al. [95] reported a direct-current (DC) sputtering system for the direct deposition of Au NPs on ZnO nanorods (Au/ZnO NRs). Initially, a radio-frequency sputtering system was employed to deposit a ZnO seed layer onto the Cr/Au film. Subsequently, ZnO nanorods with an average diameter of 54 nm and an average length of 2 μm were grown through the hydrothermal method at 90 °C. Ultimately, Au NPs were deposited onto the surface of the ZnO nanorods via DC sputtering. The addition of Au NPs enhanced the specific surface area, thereby creating more active sites for glucose oxidation. Consequently, the Au/ZnO NR electrode exhibited greater sensitivity compared to the ZnO NR electrode. In addition to noble metals, non-noble metals have also been employed in ZnO-based non-enzymatic electrochemical glucose sensors. For example, Golli et al. [96] reported Cu/ZnO nanocomposites using a sol–gel approach for non-enzymatic electrochemical glucose sensors (Figure 4d). They then coated Cu/ZnO thin films onto the surface of a GCE and immobilized them with chitosan (GHIT). The ZnO particles exhibited a size range of 22–55 nm, with an average size of 38 nm (Figure 4e). Moreover, the illuminated white particles in Figure 4f indicate the presence of copper nanoparticles (Cu NPs). Copper underwent a redox reaction involving $Cu^{2+}/Cu^{3+}/Cu^{2+}$, which facilitated the oxidation of glucose (Figure 4g). The mechanism of glucose oxidation catalyzed by Cu/ZnO is shown in Equations (3)–(7):

$$Cu + 2OH^- \rightarrow Cu(OH)_2 + 2e^- \quad (3)$$

$$Cu(OH)_2 + OH^- \rightarrow CuOOH + H_2O + e^- \quad (4)$$

$$CuOOH + C_6H_{12}O_6 \rightarrow Cu(OH)_2 + C_6H_{11}O_6 \quad (5)$$

$$C_6H_{11}O_6 + OH^- \rightarrow C_6H_{10}O_6 + H_2O + e^- \quad (6)$$

$$C_6H_{10}O_6 \rightarrow C_6H_{12}O_7 \quad (7)$$

The existence of the GHIT layer could enhance biocompatibility, while the incorporation of Cu NPs proved the advantages of augmenting the specific surface area and improving electron transport across the electrode surface.

2.5. Titanium-Based Oxides

Titanium dioxide (TiO_2), a typical semiconductor, exhibits distinctive optical and electrical properties. Moreover, TiO_2 demonstrates favorable attributes, including biocompatibility, catalytic efficiency, and non-toxicity [97–99]. As a consequence, TiO_2 finds extensive application in diverse fields, such as electrochemistry [100], photoelectrochemistry [101], electrochemiluminescence [102], and photocatalytic fuel cells [103]. To fully harness its advantages, novel morphologies of TiO_2, such as nanoribbon [104] and nanotube arrays [105], have been recently devised by scholars. Notably, in the field of electrochemical glucose sensing, researchers have enhanced the sensing performance of TiO_2 through the creation of heterojunctions or the incorporation of other materials to modify its bandgap structure.

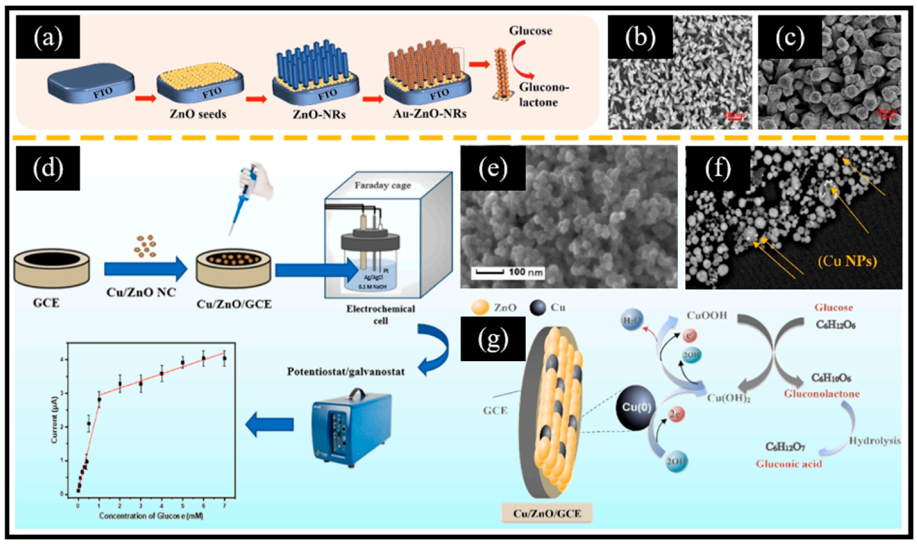

Figure 4. (**a**) Schematic diagram of the glucose sensor based on Au-ZnO NRs. SEM images of (**b**) ZnO NRs and (**c**) Au-ZnO NRs. (**d**) Schematic diagram of the glucose sensor based on Cu/ZnO/GCE. SEM images of (**e**) ZnO and (**f**) Cu/ZnO. (**g**) Schematic diagram of the Cu/ZnO/GCE sensor for glucose oxidation in an alkaline environment. (**a**–**c**) Reproduced with permission [45]. Copyright 2021, Elsevier. (**d**–**g**) Reproduced with permission [96]. Copyright 2022, Elsevier.

Chiu et al. [46] obtained Au NPs-TiO_2/PANI composites through the deposition of Au NPs and TiO_2 NPs onto a PANI substrate (Figure 5a). Initially, polyaniline was created through chronoamperometry in a solution composed of 0.5 M HCl, 0.1 M aniline monomer, and 3 M KCl. Subsequently, TiO_2 and Au NPs were deposited sequentially on the PANI support. The TiO_2 aggregated densely, covering nearly all PANI surfaces with evenly distributed Au NPs (depicted as bright white spots in Figure 5b,c). The oxidation mechanism of glucose on the active surface of Au NPs-TiO_2 is illustrated in Figure 5d. The sensor exhibited a remarkable sensitivity of 313.6 μA mM^{-1} cm^{-2} and a low LOD of 0.15 μM. Notably, the sensor displayed outstanding stability, maintaining its performance for an extended period of 70 days. These excellent sensing properties benefited from the synergistic effect of the active center and PANI substrate: (i) PANI increased the conductivity, while the large specific surface area of PANI provided abundant sites and avoided the aggregation of deposited Au NPs and TiO_2 NPs; and (ii) Au and TiO_2 as dual active centers accelerated the oxidation of glucose. Moreover, Jeong et al. [106] employed the thermal plasma method to prepare TiO_2 NPs, subsequently depositing them onto an FTO substrate. They then utilized an electrochemical approach to deposit the substrate with chitosan and polypyrrole (CS-PPy) thin films, resulting in the formation of CS-PPy/TiO_2 nanocomposites. TiO_2 NPs, with an approximate average size of 20 nm, were securely affixed to the FTO substrate via heat treatment at 450 °C for 24 h. PPy and CS were linked through hydrogen bonds, whereas the interaction between CS-PPy and TiO_2 involved both hydrogen bonds and Ti-N bonds. The electrochemical performance of the glucose sensor based on CS-PPy/TiO_2/FTO exhibited a high sensitivity of 302.0 μA mM^{-1} cm^{-2} and a low LOD of 6.7 μM. Furthermore, TiO_2 NPs produced using the thermal plasma method exhibit greater purity and a significantly larger specific surface area compared to those synthesized via the conventional sol–gel technique, which could expose more active sites and improve the sensitivity and selectivity of electrochemical glucose sensors. More interestingly, compared with disordered TiO_2 NPs, the ordered TiO_2 array structure plays an important role in increasing the specific surface area and improving the electron transfer rate. For instance, Kumar et al. [107] reported the fabrication of Cu_2O-modified TiO_2 nanotube arrays on Ti_6Al_4V alloy substrates (Ti_6Al_4V-TNTs/Cu_2O NPs) for constructing

non-enzymatic electrochemical glucose sensors to monitor glucose sensitively. Initially, the Ti_6Al_4V alloy was immersed in a solution comprising ammonium fluoride and ethylene glycol. During this process, the Ti_6Al_4V alloy plate served as the anode, while a Pt foil acted as the cathode. An anodization voltage of 20 V was applied for 3 h. Subsequently, an annealing procedure was conducted to induce the transformation of the TNTs from the amorphous to the anatase phase. To further improve the conductivity, Cu_2O was deposited onto TNTs via the chemical bath deposition method. The TNT thin plate was immersed in the $Cu(NO_3)_2{\cdot}3H_2O$ solution, followed by the addition of NaOH under continuous stirring, and then the product was annealed to obtain TNTs/Cu_2O NPs. The chemical reactions that occurred during the whole process are shown in Equations (8)–(10):

$$Cu(NO_3)_2{\cdot}3H_2O + 2NaOH \rightarrow Cu(OH)_2 + 2NaNO_3 + 3H_2O \quad (8)$$

$$Cu(OH)_2 \rightarrow CuO + H_2O \quad (9)$$

$$4CuO \rightarrow 2Cu_2O + O_2 \quad (10)$$

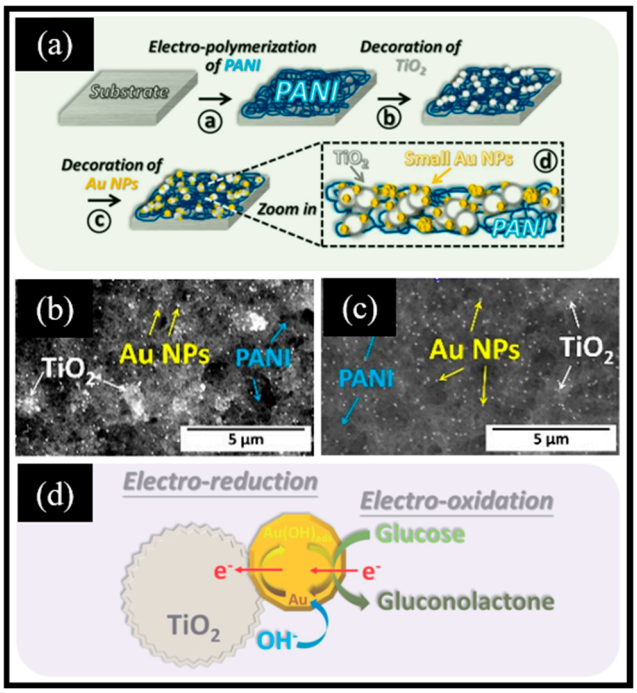

Figure 5. (**a**) Schematic illustration of the Au NPs-TiO_2/PANI composite modified electrode. SEM images of (**b**) 5 g/L TiO_2/PANI and (**c**) 0.5 g/L TiO_2/PANI; (**d**) schematic diagram of the oxidation of glucose on the Au-NPs-TiO_2 active surface. Reproduced with permission. (**a**–**d**) Reproduced with permission [46]. Copyright 2020, Elsevier.

The Cu_2O/TNT-based electrochemical glucose sensor demonstrated a wide linear range spanning from 5 mM to 35 mM, with a high sensitivity of 101.65 mA mM^{-1} cm^{-2}. These studies suggest that we can improve the electrocatalytic activity of electrode materials by (i) regulating their morphology and (ii) constructing multi-component composite materials.

2.6. Manganese-Based Oxides

Manganese dioxide (MnO_2), a typical transition metal oxide, is known for its low cost, minimal environmental impact, high catalytic activity, outstanding chemical stability, and excellent biocompatibility [108–110]. In comparison to other non-noble metal oxides, such as Cu_2O and Co_3O_4, MnO_2 possesses relatively poor electrical conductivity. To address

this limitation, researchers have enhanced the conductivity by integrating other high-conductivity materials, like CuO and PANI, to create MnO_2-based nanocomposites [47,111]. Notably, the 2D structure of MnO_2 has gained significant attention in recent years in the field of non-enzymatic electrochemical glucose sensors. This phenomenon is primarily attributed to the significant specific surface area offered by 2D MnO_2, which provides a great deal of active sites and significantly improves electrochemical redox kinetics.

The hydrothermal method for the in situ growth of 2D structures is a typical method for preparing MnO_2 nanosheets. For example, Huang et al. [112] reported a straightforward hydrothermal method for fabricating MnO_2 nanosheet arrays on nickel foam (MnO_2 NS/NF). The surface of the NF changed from smooth to rough with the addition of MnO_2. The integrated electrode constructed by the MnO_2 NS/NF three-dimensional (3D) network facilitated easy access to target molecules and exhibited strong electrical conductivity. Furthermore, the staggered growth of 2D MnO_2 nanosheets with a larger specific surface area resulted in an increased number of exposed active sites. Thus, the electrochemical non-enzymatic glucose sensor based on MnO_2 NS/NF exhibited a wide linear range from 1 μM to 1.13 mM, a high sensitivity of 6.45 mA mM^{-1} cm^{-2}, and a low LOD of 0.5 μM. Additionally, the sensor demonstrated an excellent anti-interference performance for glucose detection, even in the presence of interfering substances, such as dopamine (DA), ascorbic acid (AA), uric acid (UA), and other compounds. Interestingly, compared with the hydrothermal method, the electrodeposition technique possesses greater advantages in the controllable construction of MnO_2 nanosheets. For instance, Jadhav et al. [113] presented a technique for producing vertically aligned MnO_2 thin-film nanosheets on stainless-steel (SS) substrates using anodic potentiostatic deposition. Mn^{2+} combined with OH^- to form $Mn(OH)_2$, which was subsequently converted into MnO_2 through annealing. The average thickness of the MnO_2 flakes was 38 nm, and the separation between two neighboring flakes was approximately 50 nm. The vertically grown MnO_2 nanosheets were staggered, and the large specific surface area provided abundant active sites for electrochemical redox reactions. Moreover, the tubular structure aligned along the *c*-axis of the crystal lattice established effective pathways for ion transport, thereby minimizing resistance during electrochemical reactions. The sensor exhibited a sensitivity of 4341 μA mM^{-1} cm^{-2}, a linear range spanning from 50 μM to 1.2 mM, and a low LOD of 0.53 μM. These remarkable glucose-oxidizing abilities originate from the distinctive structure of vertically oriented MnO_2 thin-film nanosheets. Moreover, another report on the electrodeposition technique was the preparation of binary MnO_2/Co_3O_4 on the surface of electrospun carbon nanofibers (MnO_2/Co_3O_4@ECNFs) reported by Yin et al. [114]. The pure ECNFs exhibited a smooth surface, and then they were stabilized and carbonized at different temperatures. Subsequently, they were modified in an HNO_3 solution to yield ECNFs enriched with carboxyl and hydroxyl groups. The modified fibers were immersed in a mixed solution of Na_2SO_4, $MnSO_4$, and $CoSO_4$, and a certain current was applied to facilitate the deposition of Mn-Co bimetallic oxides. Compared with Co_3O_4@ECNFs and MnO_2@ECNFs, MnO_2/Co_3O_4@ECNFs displayed a more densely packed and aggregated structure. The detection mechanism of glucose catalyzed by Co_3O_4/MnO_2 is shown in Equations (11)–(13):

$$Co_3O_4 + 4OH^- \rightarrow 3CoO_2 + 2H_2O + 4e^- \quad (11)$$

$$2CoO_2 + C_6H_{12}O_6 \rightarrow 2CoOOH + C_6H_{12}O_6 \quad (12)$$

$$2MnO_2 + C_6H_{12}O_6 \rightarrow 2MnOOH + C_6H_{12}O_6 \quad (13)$$

In the presence of glucose, CoO_2 and MnO_2 were transformed into CoOOH and MnOOH, respectively, accompanying the conversion of glucose to gluconolactone. The

bimetallic oxides demonstrated stronger redox kinetics compared to single oxides, which can be attributed to the synergistic enhancement effect of Co_3O_4 and MnO_2. Furthermore, the non-enzymatic electrochemical glucose sensor based on MnO_2/Co_3O_4@ECNFs/GCE demonstrated an excellent linear relationship in two concentration ranges of 5 μM to 0.57 mM and 0.57 mM to 1.93 mM. This method for preparing multi-component metal oxides through a straightforward one-step electrodeposition technique has provided significant inspiration for our research.

Here, the reported MO-based non-enzymatic electrochemical glucose sensors are categorized according to the types of MO composites (Table 1).

Table 1. Non-enzymatic electrochemical glucose sensors based on MO composites.

Nanomaterial	Electrolyte	Sensitivity	Linear Range	LOD	Real Sample	Ref.
Fe_3O_4@Au@CoFe-LDH	1.0 M KOH	6342 μA mM^{-1} cm^{-2}	37.5 μM–15.64 mM	12.7 μM	/	[30]
Fe_3O_4 nanospheres	0.1 M NaOH	96.1 μA mM^{-1} cm^{-2} 38.2 μA mM^{-1} cm^{-2}	0 mM–10 mM 3 mM–18 mM	19.2 μM	Apple/ watermelon/ pear juice	[55]
NiO/Fe_2O_3	0.05 M PBS (pH = 7.0)	230.5 μA mM^{-1} cm^{-2}	50 μM–2.867 mM	3.9 μM	Human serum	[57]
GS/NFG/PANI/ Fe_3O_4@MIL-101-NH_2	0.02 M PBS	61.183 μA $μM^{-1}$ cm^{-2}	0.5 μM–25 mM	0.3 μM	Human plasma and serum	[43]
Co_3O_4/CeO_2	0.1 M NaOH	790.746 μA mM^{-1} cm^{-2}	83.75 μM–2.796 mM	5.5 μM	Fruit juice	[32]
Co_3O_4NPs@HCC-MWCNTs	0.1 M NaOH	1261 μA mM^{-1} cm^{-2}	0.5 μM–0.1 mM	43.9 nM	Human serum	[62]
Co_3O_4 NSs	0.1 M NaOH	2787 μA mM^{-1} cm^{-2}	1 μM–1.1 mM	0.1 μM	/	[66]
NHCN-Co_3O_4	0.1 M NaOH	12.9 μA mM^{-1} cm^{-2}	1.0 μM–32 mM	0.2 μM	Human serum	[44]
CuO/CNT	0.1 M NaOH	4340 μA mM^{-1} cm^{-2}	0.5 μM–1 mM	0.355 μM	Human urine and beverages	[72]
CuO/AC	0.1 M NaOH	2073.6 μA mM^{-1} cm^{-2}	0.2 μM–2.4 mM	0.1 μM	/	[74]
CuO@MCM-41	0.1 M NaOH	17.23 mA mM^{-1} cm^{-2}	83 μM–1.5 mM	16 nM	/	[83]
Au/Cu_2O/GQDs	0.1 M PBS (pH = 7.4)	32.5 μA $μM^{-1}$ cm^{-2}	1 nM–1 M	70 nM	/	[84]
Pt/ZnO NRs	0.1 M NaOH	32.0527 μA mM^{-1} cm^{-2}	0 mM–8 mM	/	/	[37]
B12-derived ZnO	0.1 M NaOH	78.88 mA mM cm^{-2}	1 mM–10 mM	5 μM	Human whole blood	[91]
Au/ZnO NRs	0.1 M NaOH	182.96 μA mM^{-1} cm^{-2}	0 mM–8 mM	/	/	[95]
Ag@TiO_2	0.1 M NaOH	19106 μA mM^{-1} cm^{-2} 4264 μA mM^{-1} cm^{-2}	1 μM–1 mM 1 mM–4 mM	0.18 μM	Energy beverage and beer	[104]
Ni-DLC/TiO_2 nanotube	0.5 M NaOH	1063.78 μA mM^{-1} cm^{-2}	0.99 mM–22.97 mM	0.53 μM	/	[105]
Ti_6Al_4V-TNTs/ Cu_2O NPs	0.1 M NaOH	101.65 μA mM^{-1} cm^{-2}	5 mM–35 mM	0.655 mM	Orange juice	[107]
N-htGONR/MnO_2	0.1 M PBS (pH = 7.4)	82.05 μA mM^{-1} cm^{-2}	50 μM–5 mM	8 μM	Beer	[110]
AuNPs-MnO_2/PANI	0.1 M KOH	13.1 μA mM^{-1} cm^{-2}	0.5 mM–10 mM	/	/	[47]

Note: LDHs: layered double hydroxides. GS: graphite sheet. NFG: nitrogen-doped functionalized graphene. PANI: polyaniline. NPs: nanoparticles. HCC: hollow carbon chain. NSs: nanosheets. NHCN: nitrogen-doped hollow carbon nano-polyhedron. CNTs: carbon nanotubes. AC: activated carbon. MCM-41: mobile crystalline material-41. GQDs: graphene quantum dots. NRs: nanorods. B12: vitamin B12. Ni-DLC: Ni and diamond-like modified carbon. TNTs: TiO_2 nanotubes. N-htGONRs: nitrogen-doped heat-treated graphene oxide nanoribbons.

3. MS-Based Non-Enzymatic Electrochemical Glucose Sensors

In common metal sulfides, metal atoms and sulfur atoms may exist in various atomic ratios, resulting in different phases (such as CuS, Cu_2S, CoS, Co_3S_4, NiS, Ni_3S_2, Ni_7S_6, etc.). Sulfides of the same metal, in different phases, exhibit significant differences in their catalytic performance for glucose oxidation, highlighting the need for the precise control of crystal phases. When preparing electrode materials, crystal-phase control strategies from other research areas can be referenced. (i) Reaction temperature: An increase in temperature during the reaction helps accelerate the reaction rate, crystal growth, and phase transition. (ii) Reaction time: As the reaction time increases, the crystal phase may transform from a metastable phase to a stable one. (iii) Heat treatment: Heat treatment of the synthesized product may also induce a phase transition. For example, the 2H phase of molybdenum disulfide (MoS_2), which has semiconductor properties, can transform into the

metallic 1T phase after high-temperature annealing [115]. (iv) Molar ratio of metal source to sulfur source: It is feasible to obtain the target product by artificially controlling the feed ratio of the precursors. It is important to note that when either the metal source or sulfur source is in excess relative to the other, the excess may no longer participate in the reaction. This requires the consideration of other factors, such as the reaction temperature and time. (v) Electrodeposition parameters: The crystal phases of sulfides can be controlled by adjusting the scanning rate and deposition cycle during the electrodeposition process. For example, Li et al. [116] controlled the crystal phases of Ni_xS_y grown in situ on carbon paper by adjusting the parameters of the unipolar pulse electrodeposition process. Ultimately, they obtained two different crystal phases: Ni_9S_8 and Ni_3S_2.

3.1. Copper-Based Sulfides

Copper sulfide (Cu_xS_y), a common transition-metal chalcogenide semiconductor, possesses several desirable characteristics, including stability, biocompatibility, low cost, and high catalytic activity [117,118]. Interestingly, the redox reaction between Cu (II)/Cu (III) redox pairs as electron mediators can effectively accelerate the electrocatalytic oxidation process of glucose. In the realm of non-enzymatic electrochemical glucose sensors, Cu_xS_y is frequently designed into 2D or hollow structures, capitalizing on its advantages of a large specific surface area and porosity to enhance sensing performance [119–121]. Scalability and uniformity of Cu_xS_y are important parameters for its future commercialization. Recently, Cho et al. [122,123] obtained uniform and highly crystalline CuS films on Cu foils using sulfurization methods with hydrogen sulfide gas (H_2S) or an ammonium sulfide solution. Interestingly, by adjusting parameters, such as the sulfur source concentration and sulfurization time, they obtained CuS films with different sub-microstructures. These uniform CuS films demonstrated great potential in gas sensing, temperature sensing, and thermoelectric platforms. However, the relatively poor conductivity of Cu_xS_y has hampered its extensive application in sensing. It is worthy to note that various approaches, such as integrating with noble metal-based materials and conductive polymers, have been developed to improve catalytic performance, electrical conductivity, and mechanical stability.

Mai et al. [124] reported an anodic oxidation method to prepare 2D Cu_xS (CuS and Cu_2S) nanosheets on 3D copper foam (3DCF), followed by the electrodeposition of Au NPs on Cu_xS. The 3D copper foam structure provided a large active area, and the highly conductive Cu_xS nanosheets were interconnected to form a conductive framework. Au NPs (with an average particle size in the range of 100–200 nm) were uniformly deposited on Cu_xS, effectively avoiding the aggregation of Au NPs. The non-enzymatic electrochemical glucose sensor based on the Au-Cu_xS/3DCF/GCE electrode exhibited a wide linear range of 1.98 μM–976.56 μM, along with a high sensitivity of 59 μA μM^{-1} cm^{-2}, as well as a low LOD of 7.62 μM. This excellent sensing performance was attributed to the following reasons: (i) biomolecules could be steadily immobilized by strong interaction of Au-S bondm and (ii) the synergistic effect between Au NPs and Cu_xS improved charge transfer and electrolyte penetration. In addition to noble metals, chitosan polymer-derived carbon substrates can also significantly improve electron transport at the electrode surface. For instance, Sharma et al. [125] reported a one-step hydrothermal synthesis of a composite of N and S co-doped chitosan (NSC) microspheres and CuS (CuS/NSC) for non-enzymatic electrochemical glucose sensors (Figure 6a). Firstly, a mixture containing chitosan, thiourea, copper sulfate ($CuSO_4$), formaldehyde, and acetic acid was introduced into a Teflon-lined stainless-steel autoclave and heated to 190 °C for 24 h. Secondly, the dried product was carbonized at 800 °C for 2 h under a nitrogen atmosphere. Chitosan served as the carbon and nitrogen source, while thiourea acted as the source of sulfur and nitrogen. Furthermore, the hydroxyl and amine groups in chitosan could interact with thiourea, acetic acid, and

formaldehyde to form a self-assembled network. Pure NSC showed a spherical structure (Figure 6b), and CuS nanoparticles with an average particle size in the range of 10–20 nm were distributed on the surface of NSC spheres (Figure 6c,d). NSC served as a supportive matrix for anchoring CuS nanoparticles, resulting in an enhanced electrochemical response. The linear range of this sensor spanned from 160 μM to 11.76 mM, with an LOD of 2.72 μM and a sensitivity of 13.62 mA mM^{-1} cm^{-2} (Figure 6e). Therefore, improving the dispersion of electroactive materials is an effective way to enhance the performance of non-enzymatic electrochemical glucose sensors. Recently, He et al. [48] reported a unique vine-like CuS nanowire (V-CuS NWs) for non-enzymatic electrochemical glucose sensors (Figure 6f–h). Thiourea was used as a source of sulfur, decomposing into NH_4OH and H_2S during the hydrothermal process. Subsequently, Cu^{2+} and S^{2-} in the solution reacted to form CuS nanoparticles. Interestingly, when polyethylene glycol (PEG) was added to the solution, it acted as both a template and a polymerization agent, allowing CuS nanoparticles to attach to its surface and form unique nanowire structures. Consequently, the nanowires were cross-linked to form a 3D network structure. The current response of the non-enzymatic electrochemical glucose sensor based on V-CuS NWs demonstrated good linear relationship versus glucose concentration in the range of 1 μM to 7 mM (Figure 6i,j). In addition, the sensor exhibited excellent anti-interference and stability (Figure 6k,l). Therefore, when preparing MS-based nanomaterials, we should consider designing them into 2D or 3D structures to expose more active sites and shorten the electron transport channel.

3.2. Molybdenum-Based Sulfides

Molybdenum disulfide (MoS_2), a typical chalcogenide, possesses a unique 2D layered structure, adjustable band gap (≈1.8–1.9 eV), and good mechanical stability, which has triggered a research boom in the fields of biosensors, electrocatalysis, and supercapacitors [126–129]. However, the relatively poor electrical conductivity and electrocatalytic activity toward glucose of pure MoS_2 limit the application of MoS_2-based non-enzymatic electrochemical glucose sensors. Therefore, introducing other semiconductors to construct MoS_2-based heterojunctions is an effective strategy to overcome the abovementioned problems.

As mentioned in Section 3.1, the Cu (II)/Cu (III) redox pair of Cu_xS_y is beneficial for catalyzing the oxidation of glucose. Therefore, researchers usually combine Cu_xS_y with MoS_2 as the electroactive material of MoS_2-based non-enzymatic electrochemical glucose sensors. Recently, Cao et al. [49] used Cu_2O cubes as a sacrificial template; dopamine, sodium molybdate, and thioacetamide as the carbon source, Mo source, and S source, respectively; and then obtained MoS_x-supported hollow Cu_9S_5/C (Cu_9S_5/C/MoS_x) by high-temperature carbonization and a hydrothermal reaction (Figure 7a). During the sulfurization process, O^{2-} and S^{2-} undergo ion exchange reactions, resulting in the transformation of solid Cu_2O cubes into hollow Cu_9S_5 frameworks (Figure 7b,c). Furthermore, compared to Cu_2O and Cu_2O/C, Cu_9S_5/C/MoS_x exhibited a better ability to catalyze glucose oxidation. Moreover, Sharma et al. [130] used a one-step hydrothermal method to prepare CuS/MoS_2 (Figure 7d,e) for a non-enzymatic electrochemical glucose sensor. Thiourea ($(NH_2)_2CS$) was used as the sulfur source and reacted with Cu^{2+} and $MoO_4{}^{2-}$ in an alkaline solution, as shown in Equations (14)–(16):

$$(NH_2)_2CS + 2OH^- \rightarrow S^{2-} + 2H_2O + H_2CN_2 \quad (14)$$

$$Cu^{2+} + S^{2-} \rightarrow CuS\downarrow \quad (15)$$

$$4MoO_4{}^{2-} + 15(NH_2)_2CS + 6H_2O \rightarrow 4MoS_2\downarrow + SO_4{}^{2-} + 6SCN^- + 24NH_3 + 9CO_2\uparrow \quad (16)$$

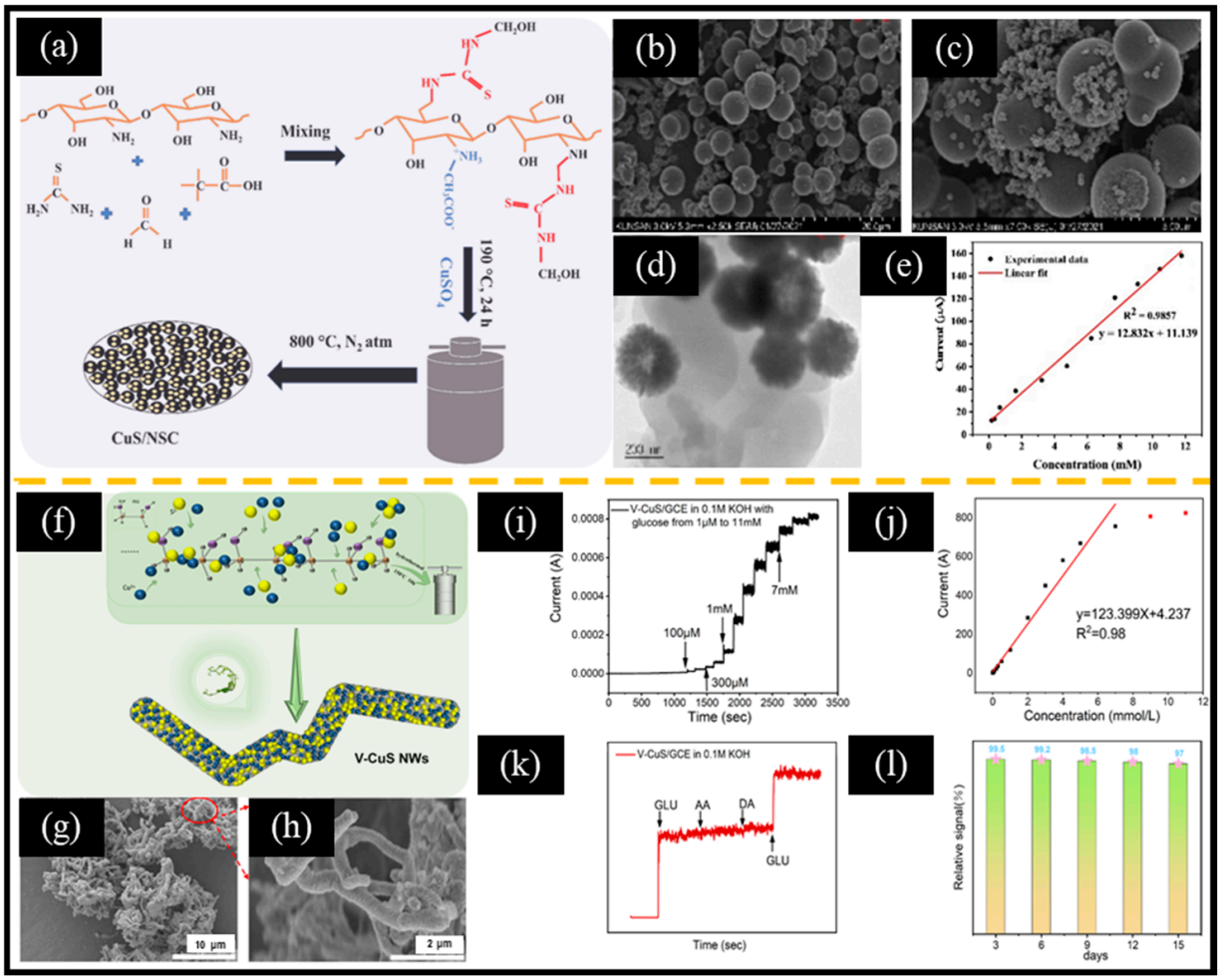

Figure 6. (**a**) Schematic diagram of the preparation of CuS/NSC. SEM images of (**b**) NSC and (**c**) CuS/NSC. (**d**) TEM image of CuS/NSC. (**e**) Calibration curve of current response vs. glucose concentration. (**f**) Schematic diagram of the synthesis of V-CuS NWs. SEM images of (**g**,**h**) V-CuS NWs. (**i**) Response current to continuous addition of glucose and corresponding (**j**) calibration plot of current versus glucose concentration. (**k**) Anti-interference and (**l**) stability test. (**a**–**e**) Reproduced with permission [125]. Copyright 2022, Elsevier. (**f**–**l**) Reproduced with permission [48]. Copyright 2024, Elsevier.

It is noteworthy that CuS/MoS_2 exhibited excellent electrocatalytic activity due to (i) sufficient activity sites from the increased surface area and (ii) the synergistic effect of CuS and MoS_2 (Figure 7f). Therefore, the CuS/MoS_2-based non-enzymatic electrochemical glucose sensor showed a wide linear range of 0.1 mM-11 mM, a high sensitivity of 252.7 μA mM^{-1} cm^{-2}, and a low LOD of 1.52 nm (Figure 7g). The above two works suggest that we should make full use of the large specific surface area of 2D-MoS_2 when preparing MoS_2-based composite materials. More interestingly, Luo et al. [131] constructed a non-enzymatic electrochemical glucose sensor based on an MoO_3-MoS_2/Ni porous array/screen-printed electrode (SPE) using polystyrene spheres as sacrificial templates through a two-step electrodeposition method (Figure 7h). Due to the large specific surface area and abundant active sites supported by the porous array, significant synergistic effects of MoO_3 and MoS_2, and the excellent conductivity of the Ni array, the MoO_3-MoS_2/Ni array showed a higher current response than the Ni array, MoO_3/Ni array, and MoO_3-MoS_2/Ni film (Figure 7i). This strategy of constructing a multi-component, ordered array structure by a simple electrodeposition method is valuable for reference.

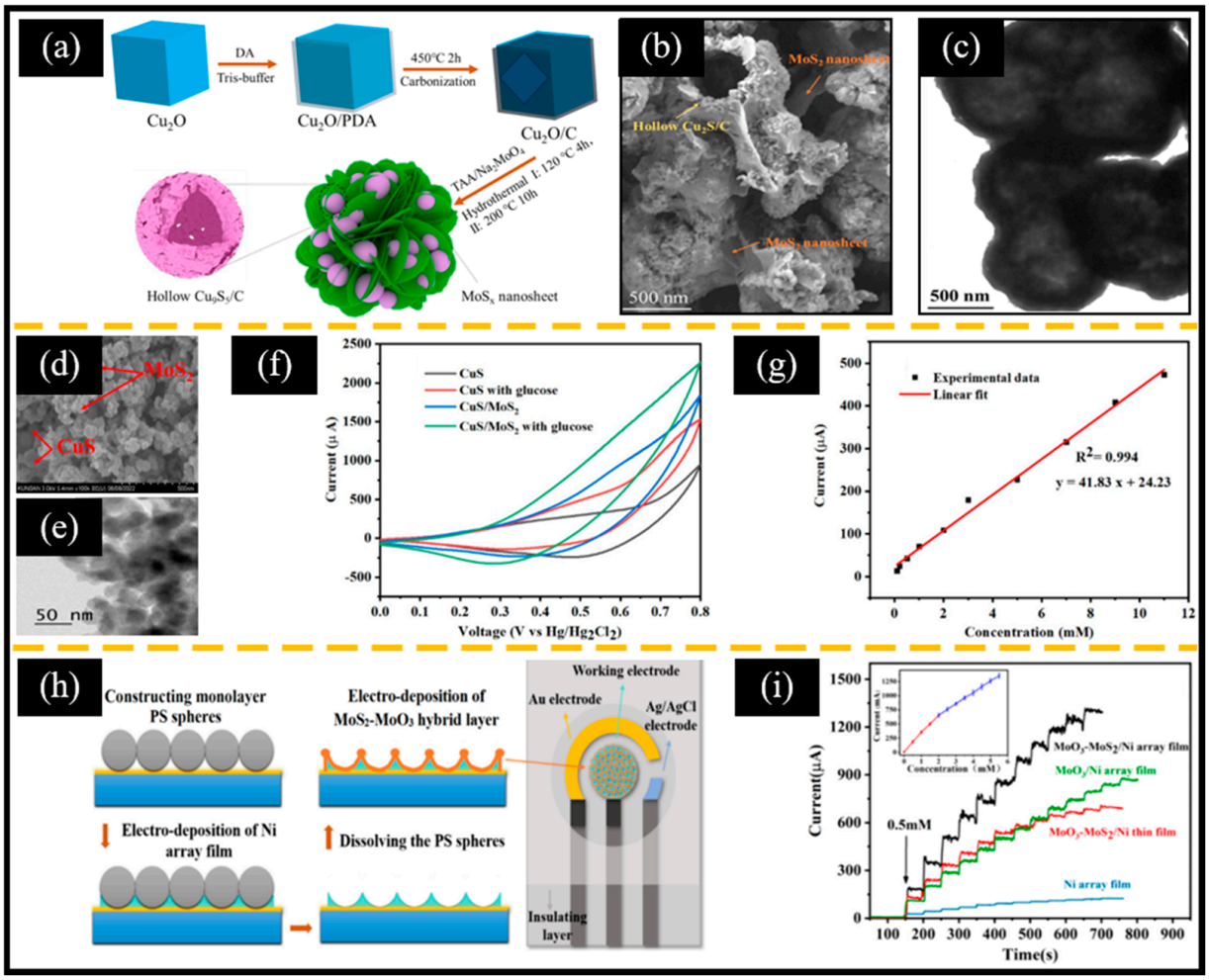

Figure 7. (**a**) Schematic diagram of the preparation of $Cu_9S_5/C/MoS_x$. (**b**) SEM and (**c**) TEM images of $Cu_9S_5/C/MoS_x$. (**d**) SEM and (**e**) TEM images of CuS/MoS_2. (**f**) CV spectra with and without glucose. (**g**) Calibration curve of current response vs. glucose concentration. (**h**) Schematic diagram of screen-printed electrodes based on MoO_3-MoS_2/Ni porous arrays. (**i**) Typical i-t curve of the MoO_3-MoS_2/Ni electrode following successive additions of glucose in 0.2 M of NaOH (inset: calibration curve of current response vs. glucose concentration). (**a**–**c**) Reproduced with permission [49]. Copyright 2024, Elsevier. (**d**–**g**) Reproduced with permission [130]. Copyright 2024, Cell Press. (**h**,**i**) Reproduced with permission [131]. Copyright 2023, Elsevier.

3.3. Cobalt-Based Sulfides

Cobalt sulfide (Co_xS_y) is a significant semiconductor nanomaterial with attributes including cost-effectiveness, a straightforward preparation process, high conductivity, favorable biocompatibility, and rapid redox kinetics [132,133]. Furthermore, cobalt sulfide exists in various chemical states (e.g., CoS, CoS_2, Co_3S_4, and Co_9S_8), showing great potential for glucose oxidation. However, pure cobalt sulfides often exhibit poor conductivity. Therefore, cobalt sulfides are usually compounded with carbon materials (such as rGO and MWCNTs) or conductive polymers (such as PPy) to enhance their conductivity. More interestingly, the combination of Co_xS_y with MOF or MOF-derived Co_xS_y has become a new strategy to construct Co_xS_y-based composites.

Sridhar et al. [134] reported a microwave synthesis method to immobilize carbon-coated CoS_2 nanoparticles on rGO (CoS_2@C-rGO). The 2D-sheet shape of graphene oxide (Figure 8a) demonstrated a large specific surface area. Cobalt acetate and thioacetamide were mixed in a graphene oxide aqueous solution at a mass ratio of 1:2 and then ultra-sonicated. After evaporating the water via hydrothermal treatment, the CoS_2@C-rGO

powder was obtained through microwave irradiation. Among them, rGO served as both a conductive platform and a suitable substrate for immobilizing cobalt sulfide nanoparticles (20–40 nm, Figure 8b), enabling the creation of unique 3D structures. The CoS_2@C-rGO-FTO electrode-based non-enzymatic electrochemical glucose sensor displayed an excellent linear response and a low LOD of 0.078 µM in the glucose range up to 3 mM. The sensor also demonstrated an outstanding anti-interference performance in the presence of UA and AA interference substances (Figure 8c). In addition to carbon-based materials, conductive polymers are also often used to enhance electron transport on electrode surfaces. For example, Qi et al. [135] reported a CoS-PPy-CP flexible electrode-based non-enzymatic electrochemical glucose sensor. Initially, PPy-CP was prepared by depositing PPy on conductive carbon paper (CP) using cyclic voltammetry. Then, CoS was grown in situ on PPy-CP by the hydrothermal method. Interestingly, CoS without PPy showed a short rod structure (CoS-CP), while CoS with PPy formed nanoparticles (CoS-PPy-CP). The roles of PPy were as follows: (i) The deposition of PPy on the CP formed a large number of folded structures, providing more sites for the growth of CoS; (ii) The -NH- coordination in PPy allowed Co^{2+} to combine with PPy; and (iii) The addition of PPy increased conductivity, which helped increase the sensitivity of the non-enzymatic electrochemical glucose sensor. The sensor showed a wide linear range in the concentration ranges of 0.5 µM–465.5 µM and 565.5 µM–8415.5 µM, while achieving a low LOD of 0.14 µM. In addition, combining Co_xS_y with MOF has become a new method to obtain Co_xS_y-based composite materials. This approach not only enhances the porosity of the composite materials, but also significantly increases their specific surface area, conductivity, and stability. For instance, Ramesh et al. [50] successfully obtained CoS@Co-MOF composites for supercapacitors and non-enzymatic electrochemical glucose sensors through a one-step hydrothermal method (Figure 8d). It is worth noting that the CoS@Co-MOF/GCE-based non-enzymatic electrochemical glucose sensor exhibited a wide linear range of 5 µM–1170 µM (Figure 8e). Moreover, Gharani et al. [136] reported an Ag/MoS_2@Co_3S_4 composite derived from Mo-doped ZIF-67. Surprisingly, the deposition of Ag nanoparticles significantly reduced the charge transfer resistance and enhanced the glucose oxidation ability. This inspires us to consider the following two points when preparing MOF-derived materials: (i) doping other metals into the MOF precursor, and (ii) introducing noble metal nanoparticles.

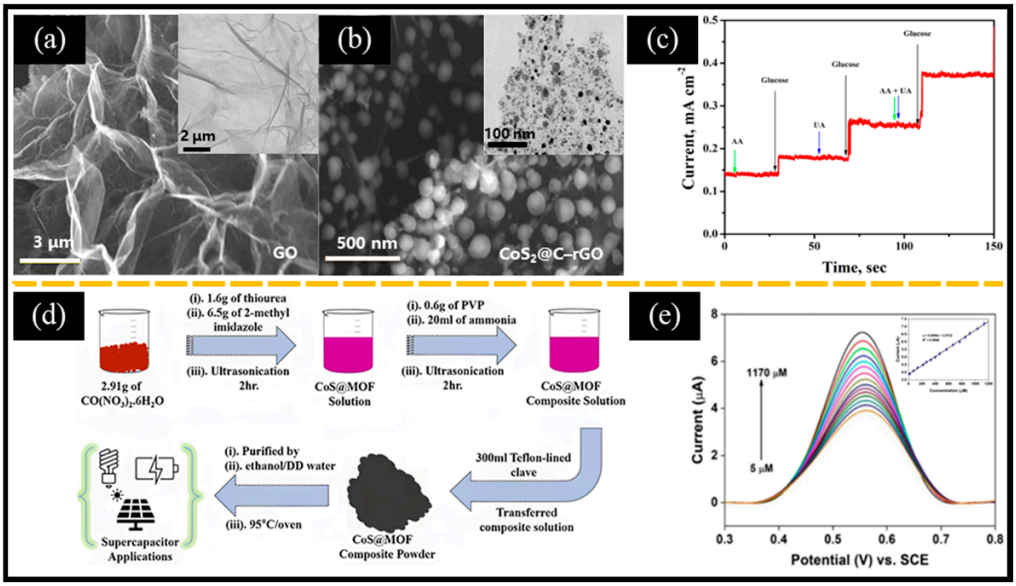

Figure 8. SEM images of (**a**) GO (inset: corresponding TEM image) and (**b**) CoS_2@C-rGO (inset: corresponding TEM image). (**c**) Amperometric response showing the anti-interference immunity of

the CoS_2@C-rGO-FTO electrode with 0.15 mM of UA and AA in a 0.1 M NaOH solution at the applied potential of 0.5 V. (**d**) Schematic of the preparation process of CoS@MOF for supercapacitors and non-enzymatic electrochemical glucose sensors. (**e**) DPV curves of different concentrations of glucose (inset: calibration curve of current response vs. glucose concentration). (**a**–**c**) Reproduced with permission [134]. Copyright 2018, Elsevier. (**d**,**e**) Reproduced with permission [50]. Copyright 2023, Elsevier.

3.4. Nickel-Based Sulfides

Nickel-based sulfide (Ni_xS_y) occurs in various atomic ratios, such as NiS, NiS_2, Ni_3S_2 and Ni_7S_6. The active center for effective electrochemical sensing is commonly attributed to the Ni (ii)/Ni (iii) redox pair [137,138]. Currently, Ni_xS_y with varying morphologies, including nanoparticles [139], nanospheres [140], and microspheres [141], are employed as electrode modifiers. Nevertheless, pure Ni_xS_y suffers from poor mechanical stability and low electrical conductivity [142]. Consequently, it is a great challenge to develop Ni_xS_y-based nanomaterials capable of substantially enhancing the electrochemical sensing performance. Kannan et al. [143] reported a core–shell nanowire composite consisting of Ni-Ni_3S_2/$NiMoO_4$. Cyclic voltammetry tests revealed that the electrochemical glucose oxidation behavior of Ni-Ni_3S_2/$NiMoO_4$ was significantly improved compared to Ni foam, Ni-Ni_3S_2, and Ni-$NiMoO_4$ due to the synergistic effect of different components.

As mentioned earlier, the morphology of electroactive materials affects their specific surface area (corresponding to the number of active sites) and the distance of electron transport. For example, Kim et al. [144] successfully grew Ni_3S_2 with different morphologies on nickel foam using the hydrothermal method by adjusting the volume ratio of ethanol and water (Et/W) to alter the polarity of the solution. As the water content increased, Ni_3S_2 gradually evolved from flakes to cauliflower-like microspheres and dendrites. Interestingly, the cauliflower-like Ni_3S_2 obtained at Et/W = 1:1 exhibited the lowest charge transfer resistance and the best electrochemical redox behavior. In addition to morphology, Mazurków et al. [145] recently reported that the energy band structure of electrode materials significantly influences sensitivity and selectivity in glucose detection. Specifically, they synthesized four spherical materials (CuS, Ag_2S, FeS_2, and α-NiS) of comparable sizes using wet chemical methods (Figure 9a–d). Interestingly, among the non-enzymatic electrochemical glucose sensors based on these four sulfides, the sensitivities of FeS_2, Ag_2S, CuS, and α-NiS demonstrated a gradually increasing trend. Theoretical calculations indicated that CuS and α-NiS possess moderate d-band center positions, while Ag_2S exhibited a lower d-band center, and FeS_2 exhibited a higher d-band center. Furthermore, all four sulfides exhibited a good capability to catalyze glucose oxidation (Figure 9e–h). Although α-NiS exhibited the highest sensitivity to glucose, it demonstrated the lowest selectivity. This phenomenon indicates that the influence of band structure should be taken into account when designing Ni_xS_y-based nanomaterials.

The poor conductivity of Ni_3S_2 significantly restricts its application in non-enzymatic electrochemical glucose sensors. Incorporating carbon materials or conductive polymers has been demonstrated to be an effective method for enhancing the electron transport properties of Ni_3S_2. For instance, Li et al. [51] reported a bamboo-like nitrogen-doped carbon nanotube-encapsulated nickel sulfide crystal (Ni_3S_2@NCNT) (Figure 9i). When the product obtained by refluxing nickel nitrate and dicyandiamide (DCD) was annealed, the nickel nanoparticles generated during the pyrolysis process could induce the conversion of DCD into NCNT while being encapsulated in the NCNT structure (Ni@NCNT, Figure 9j). After hydrothermal sulfurization treatment, Ni@NCNT was transformed into Ni_3S_2@NCNT, preserving its bamboo-like structure (Figure 9k–m). Interestingly, the bamboo-like structure of NCNTs enhanced electron transfer at the electrode surface while providing a robust enclosure that confined the Ni_3S_2 active centers and mitigated their aggregation.

Therefore, the non-enzymatic electrochemical glucose sensor based on Ni_3S_2@NCNT exhibited notable glucose oxidation activity within the range of 0.46 μM to 3.19 mM, with an LOD of 0.14 μM and an impressive sensitivity of 1447.64 μA mM^{-1} cm^{-2}. Moreover, Meng et al. [146] reported a nanoworm-like Ni_3S_2 on a GCE modified with hybrid films of poly 3,4-ethylenedioxythiophene-rGO (Ni_3S_2 NWs/PEDOT-rGO HFs/GCE) using electrodeposition technology for non-enzymatic electrochemical glucose sensors. Specifically, a PEDOT-rGO hybrid film was initially electrodeposited on the surface of the GCE through cyclic voltammetry in a mixed solution of an EDOT monomer and GO. Subsequently, Ni_3S_2 NWs were electrodeposited in a similar manner, employing $NiCl_2$ as the source of nickel and $(NH_2)_2CS$ as the sulfur source. The associated reaction process is shown in Equations (17) and (18):

$$Ni^{2+} + (NH_2)_2CS \rightarrow [Ni(NH_2)_2CS]^{2+} \quad (17)$$

$$3[Ni(NH_2)_2CS]^{2+} + 6e^- \rightarrow Ni_3S_2 + 2CN^- + 2NH^{4+} + (NH_2)_2CS \quad (18)$$

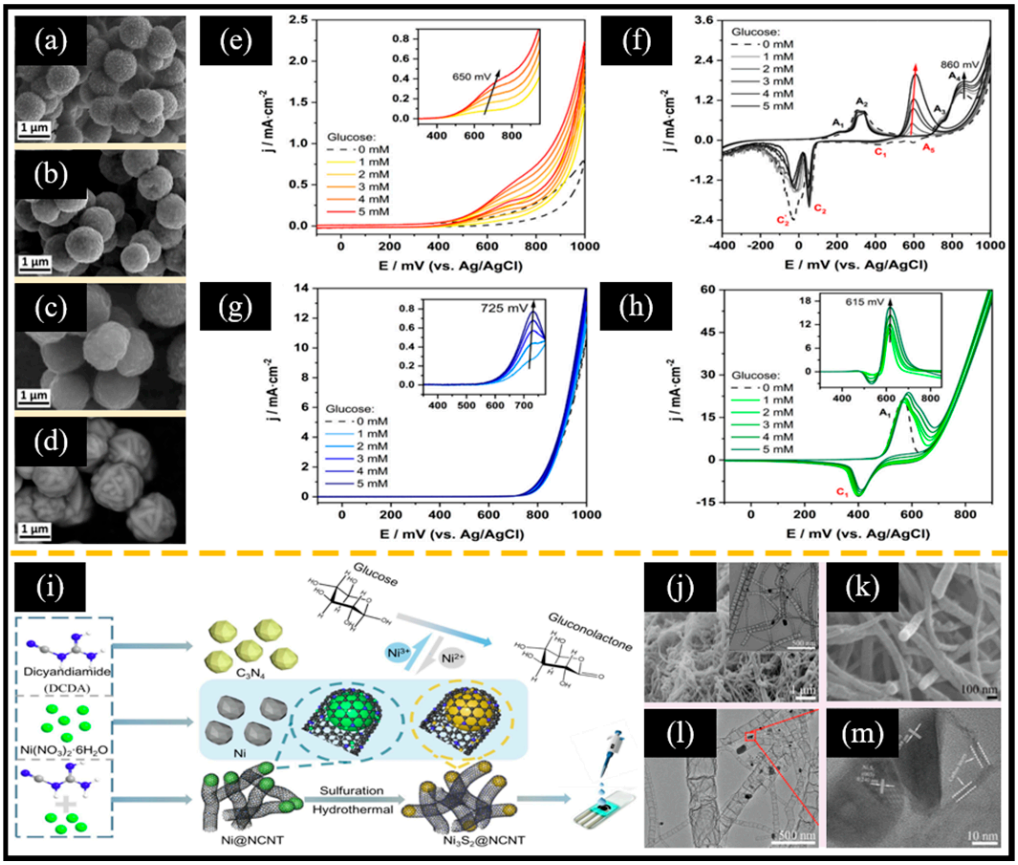

Figure 9. SEM images of (**a**) CuS, (**b**) Ag_2S, (**c**) FeS_2, and (**d**) α-NiS. CV curves of (**e**) GCE/CuS, (**f**) GCE/Ag_2S, (**g**) GCE/FeS, and (**h**) GCE/α-NiS-based non-enzymatic electrochemical glucose sensors at different glucose concentrations at a scan rate of 100 mV/s. (**i**) Illustration of the synthesis process of Ni_3S_2@NCNT. SEM images of (**j**) Ni@NCNT (inset: corresponding TEM image) and (**k**) Ni_3S_2@NCNT. (**l**) TEM image and (**m**) HRTEM image of Ni_3S_2@NCNT. (**a**–**h**) Reproduced with permission [144]. Copyright 2024, Elsevier. (**i**–**m**) Reproduced with permission [51]. Copyright 2022, Elsevier.

The non-enzymatic electrochemical glucose sensor based on Ni_3S_2 NWs/PEDOT-rGO HFs/GCE exhibited high sensitivity (2123 μA mM^{-1} cm^{-2}), a wide linear range (15 μM–9105 μM), and a low LOD (0.48 μM). The redox reaction between Ni (II) and Ni (III) at the Ni active center facilitated the oxidation of glucose. In conclusion, the regulation of

morphology and composition through various methods is an effective strategy to improve the electrochemical redox capability of nickel sulfide-based nanomaterials.

Here, the reported MS-based non-enzymatic electrochemical glucose sensors are categorized according to the types of MS composites (Table 2).

Table 2. Non-enzymatic electrochemical glucose sensors based on MS composites.

Nanomaterial	Electrolyte	Sensitivity	Linear Range	LOD	Real Sample	Ref.
CuS-NWAs	0.1 M NaOH	2610 μA mM^{-1} cm^{-2}	0.5 μM–560 μM	17.5 nM	Human serum	[119]
H-Ni$(OH)_2$@CuS	0.1 M NaOH	2738.57 μA mM^{-1} cm^{-2}	10 μM–6.64 mM	3.3 μM	Human serum	[120]
CuS NCs@Ni_1Co_2 LDHs	0.1 M NaOH	2236.4 μA mM^{-1} cm^{-2}	1 μM–4.6 mM	0.18 μM	Human serum	[121]
CuS/NSC	0.1 M NaOH	13.62 mA mM^{-1} cm^{-2}	160 μM–11.76 mM	2.72 μM	Human serum	[125]
V-CuS NWs	0.1 M KOH	2518 μA mM^{-1} cm^{-2}	1 μM–7 mM	0.13 μM	/	[48]
NiO NS-MoS_2	0.1 M NaOH	1880 μA mM^{-1} cm^{-2}	5 μM–370 μM	3.53 μM	Artificial urine and ORS	[40]
Cu_9S_5/C/MoS_x	0.1 M NaOH	2528.6 μA mM^{-1} cm^{-2} 1185.7 μA mM^{-1} cm^{-2}	0.5 μM–1.082 mM 1.082 mM–8.332 mM	0.12 μM	Human serum and beverages	[49]
CuS/MoS_2	0.1 M NaOH	252.7 μA mM^{-1} cm^{-2}	0.1 mM–11 mM	1.52 μM	Human serum	[130]
MoS_2-MoO_3/Ni	0.2 M NaOH	2278.2 μA mM^{-1} cm^{-2} 1421.1 μA mM^{-1} cm^{-2}	0.5 μM–2 mM 2 mM–5.5 mM	0.2 μM	Glucose drinks and serum	[131]
Co_3S_4	0.2 M NaOH	346.7 μA mM^{-1} cm^{-2}	2 μM–1.11 mM	0.17 μM	/	[24]
CuS/CoS	0.1 M NaOH	314.85 μA mM^{-1} cm^{-2}	0.1 mM–11 mM	1.71 μM	Human serum	[41]
Co_3S_4/$CuCo_2O_4$	0.1 M NaOH	1062.5 μA mM^{-1} cm^{-2} 512.5 μA mM^{-1} cm^{-2}	1 μM–0.405 mM 405 μM–5.03 mM	2.1 μM	Human serum and seawater	[133]
CoS@Co-MOF	0.1 M KOH	4.6 μA μM^{-1} cm^{-2}	5 μM–1.17 mM	0.11 μM	Human serum	[50]
Ag/MoS_2@Co_3S_4	0.1 M NaOH	546.8 μA mM^{-1} cm^{-2}	0.2 μM–30 μM	0.08 μM	/	[136]
NC-NiS@NS-NiS	1.0 M KOH	54.6 μA mM^{-1} cm^{-2}	20 μM–5 mM	8.3 nM	Human urine and serum	[42]
Ni_7S_6/NiO	0.1 M NaOH	7.10 μA mM^{-1} cm^{-2}	90 μM–3.12 mM	0.3 μM	Human serum	[137]
Ni-Ni_3S_2/$NiMoO_4$	0.5 M NaOH	10.49 μA μM^{-1} cm^{-2}	0 μM–0.24 mM	55 nM	Human serum	[143]
Ni_3S_2@NCNT	0.1 M NaOH	1447.64 μA mM^{-1} cm^{-2}	0.46 μM–3.19 mM	0.14 μM	Artificial sweat	[51]
Ni_3S_2 NWs/PEDOT-rGO HFs	0.1 M NaOH	2123 μA mM^{-1} cm^{-2}	15 μM–9105 μM	0.48 μM	Human serum	[146]

Note: NWAs: nanowall arrays. H-Ni$(OH)_2$: hollow Ni$(OH)_2$. CuS NCs: CuS nanocages. NSCs: N-and S-doped carbon spheres. V-CuS NWs: vine-like CuS nanowires. NiO NS: NiO nanosheet. NC-NiSs: NiS nanoclusters. NS-NiS: NiS nanosphere. NWs: nanoworms. PEDOT: poly (3,4-ethylenedioxythiophene). HFs: hybrid films. ORS: oral rehydration solution.

4. Challenges Faced by Non-Enzymatic Electrochemical Glucose Sensors in Practical Applications

Enzyme sensors typically operate under milder conditions and are sensitive to environmental factors, such as temperature, pH, and humidity. Additionally, the enzyme activity may decline over time, leading to a shorter sensor lifespan. Non-enzyme sensors, on the other hand, do not rely on enzyme activity and are expected to maintain stability under a wider range of temperatures and pH values. However, the non-enzymatic electrochemical glucose sensors reported in laboratories (including but not limited to those shown in Tables 1 and 2) almost all operate in neutral to alkaline environments, as the catalytic process requires the consumption of OH^-, which requires additional pretreatment [147,148]. Figure 10 distinguishes the differences between enzyme-based and non-enzyme electrochemical glucose sensors in various aspects. Although there is great anticipation for non-enzyme electrochemical glucose sensors, enzyme sensors are still widely used in practical applications. The path to widespread the commercialization of non-enzyme electrochemical glucose sensors remains long.

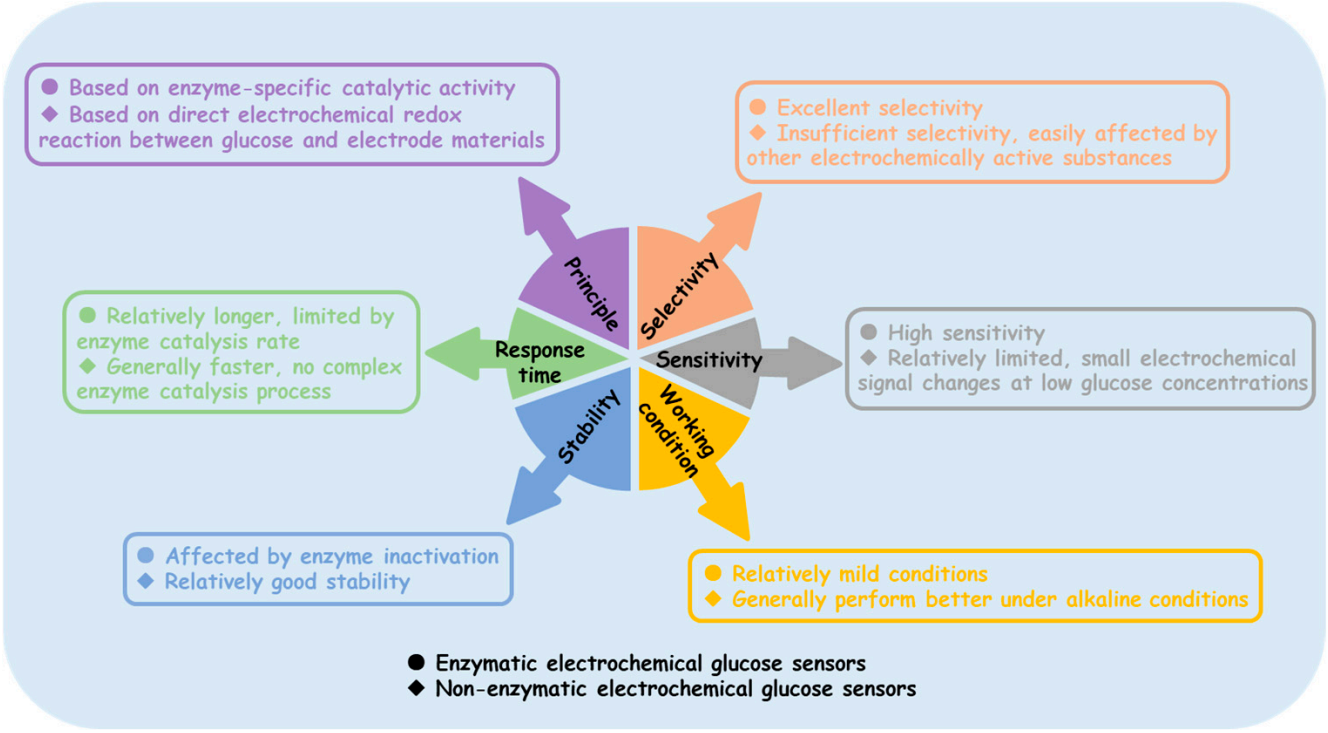

Figure 10. Comparison of enzymatic and non-enzymatic electrochemical glucose sensors.

(i) Insufficient selectivity: Non-enzyme electrochemical glucose sensors rely on the electrochemical oxidation of glucose. However, other electrochemically active substances present in complex biological samples and real-world detection environments, such as ascorbic acid (AA), uric acid (UA), and dopamine, may also undergo reactions on the electrode surface, generating interference signals that affect the accurate detection of glucose. Therefore, the selectivity of non-enzyme electrochemical glucose sensors remains a significant challenge.

(ii) Sensitivity requires further improvement: In certain applications involving low glucose concentrations, such as blood glucose monitoring in diabetic patients after insulin administration or cell cultures sensitive to glucose levels, non-enzyme glucose sensors may fail to provide accurate detection.

(iii) Limited working environment: A large number of studies have shown that common MOs and MSs exhibit good catalytic activity in alkaline environments; however, their catalytic activity significantly decreases in neutral or acidic environments.

(iv) Process optimization issues: In this review, we found that some MOs perform better after high-temperature annealing, while MSs typically involve a sulfide reaction between the metal and sulfur source. Therefore, synthesizing these materials in the laboratory generally requires high-temperature equipment, such as muffle furnaces, vacuum tube furnaces, and electric ovens. Simplifying the synthesis process would facilitate the promotion of large-scale applications.

Targeting the selectivity of non-enzymatic glucose sensors remains a major challenge for their commercialization, and we have summarized several strategies to address this challenge.

(i) Nanoconfinement effect: The fixed size of nanopores provides a strategy for excluding the influence of certain interfering substances. Benedetti et al. [149] recently reported a conductive mesoporous carbon shell-coated Au nanoparticle used to simulate the 3D structure of enzymes. The separated nanopores created the surface of Au, which

not only creates an alkaline environment for non-enzymatic detection locally, but also eliminates the interference from Cl^-, UA, AA, and proteins. This non-enzymatic electrochemical glucose sensor based on the nanoconfinement effect enables glucose detection in whole blood.

(ii) Defect engineering: Defect engineering has been demonstrated to be an effective strategy to enhance the catalytic activity of nanomaterials. Zhong et al. [150] obtained $Ni(OH)_2$ nanosheets with varying defect (oxygen vacancy) concentrations by treating the product with Ar plasma for different times. Interestingly, defective $Ni(OH)_2$ exhibited better selectivity than pristine $Ni(OH)_2$.

(iii) Design electrode materials with a stronger glucose molecule adsorption capability based on theoretical calculations: In principle, the stronger the electrode material's adsorption capability for glucose molecules, the more beneficial it is for reducing the diffusion energy barrier and accelerating reaction kinetics. Furthermore, the glucose molecule adsorption layer formed on the electrode surface hinders other interfering substances from approaching the electrode surface to some extent, thereby reducing their adsorption and reaction on the electrode.

(iv) Intelligent back-propagation (BP) neural network: Recently, Zhou et al. [151] innovatively introduced an intelligent BP neural network into electrochemical microarrays to improve the selectivity of non-enzymatic electrochemical sensors. They prepared three non-enzymatic electrodes (NiO/Pt, $Ni(OH)_2$/Au, and $Ni(OH)_2$/Pt) by electrodeposition and dripping, and then integrated them into a single electrochemical unit. This strategy overcame the overlapping oxidation peaks of glucose and lactate for the first time and can identify multiple biomarkers, which will help promote the commercialization of non-enzymatic glucose sensors in the future.

5. Summary and Prospectives

This review summarizes the recent research progress in non-enzymatic electrochemical glucose sensors based on MOs and MSs, with a primary focus on two main aspects: material synthesis methods and sensing performance. Although noble metal nanomaterials possess excellent electrical conductivity, catalytic performance, and biocompatibility, their high cost limits their application. In contrast, MOs and MSs have attracted much attention in the field of non-enzymatic electrochemical glucose sensors due to their abundant raw material reserves, simple synthesis, controllable morphology, and superior catalytic performance. Scholars are committed to developing electrode materials with outstanding catalytic activity. Therefore, various processes for synthesizing MOs or MSs have been developed, including the hydrothermal method, ultrasonic stripping method, ion exchange method, thermal reduction method, emulsion cross-linking method, vacuum spray method, micro-plasma method, electrochemical deposition method, and so on. The constructed non-enzymatic electrochemical glucose sensors based on MOs or MSs and their composites usually possess the advantages of high sensitivity, a wide linear range, low limit of detection, good selectivity, and anti-interference ability. The hydrothermal method and thermal reduction method both involve high temperature and pressure; the vacuum spray method relies on a vacuum environment; the micro-plasma method has both high equipment costs and complexity; and the ultrasonic stripping method has a low cost and process complexity, but it is primarily effective for preparation of 2D materials. The emulsion cross-linking method generally does not require high-temperature conditions, but requires precise control over the concentration of cross-linking agents and reaction conditions. The ion exchange method has moderate costs (requiring certain chemical reagents) and process complexity. From the perspectives of cost and process complexity, the electrochemical deposition method offers

economic benefits, simplicity, customizability, and suitability for large-scale production, making it a technique with significant application potential.

Currently, two primary strategies are employed to enhance the performance of non-enzymatic electrochemical glucose sensors. One strategy is to increase the porosity and specific surface area of the electrode materials by altering their morphology and structure. Larger porosity helps provide more channels for ion diffusion and reduces the ion transport distance. Larger specific surface area is beneficial for exposing more active sites, thereby improving the sensitivity of the sensor. In addition to the 2D nanosheet structures and MOF-derived porous structures we mentioned earlier, laser-induced graphene (LIG) has recently been widely used to construct electrode materials with 3D porous structures, large specific surface areas, and excellent conductivity. For example, Zhu et al. [152] reported an LIG electrode coated with Ni and Au for non-enzymatic electrochemical glucose sensors, which exhibited higher sensitivity in a relatively mild alkaline solution (pH = 10) compared to stronger alkaline solutions reported in the literature. This can be achieved through the design of morphologies (including nanotubes, nanosheets, and nanoflowers) and structures (containing a hollow, core–shell array as well as other structures). The other strategy is to form composite materials by introducing other components: (i) loading noble metal nanoparticles, such as Au, Pt, and Ag; (ii) hybridization with carbon materials, like MWCNTs, GO, and CNFs, or with conductive polymers, such as PPy, PANI, and PEDOT; and (iii) introducing other MOs or MSs to construct heterojunctions.

In addition, with the development of flexible materials, the research on glucose monitoring systems based on electrochemical sensing platforms and wearable electronic devices has become a new hotspot. Shamili et al. [153] used MWCNT, PEDOT: PSS (polystyrene sulfonate), and Fe_3O_4 nanoparticles to prepare flexible screen-printed electrodes, which were then modified with Prussian blue nanoparticles and GO_X. The designed flexible wearable sensor demonstrated reliability in detecting glucose levels in the sweat of volunteers before and after meals (Figure 11a–c). Shrestha et al. [154] developed a self-adhesive hydrogel for sweat glucose monitoring that does not require any other adhesives or surface treatments (Figure 11d–g). The key indicators for designing wearable non-enzymatic electrochemical glucose sensors include cost, comfort (e.g., weight, size, flexibility, elasticity, and minimal skin irritation), functionality (e.g., low power consumption and waterproofing), and reliable signal transmission and processing (e.g., fast response, smart interconnection, high sensitivity, selectivity, and anti-interference capabilities). Microelectromechanical systems (MEMS) technology possesses the characteristics of miniaturization, lightweight, high integration, mass production, low cost, and multi-functionality. MEMS can be easily integrated into wearable devices, paving the way for the development of wearable non-enzymatic electrochemical glucose sensors [155]. It is foreseeable that the next generation of non-enzymatic electrochemical glucose sensors is expected to advance toward miniaturization and wearability, thereby achieving rapid, painless, and real-time blood sugar detection.

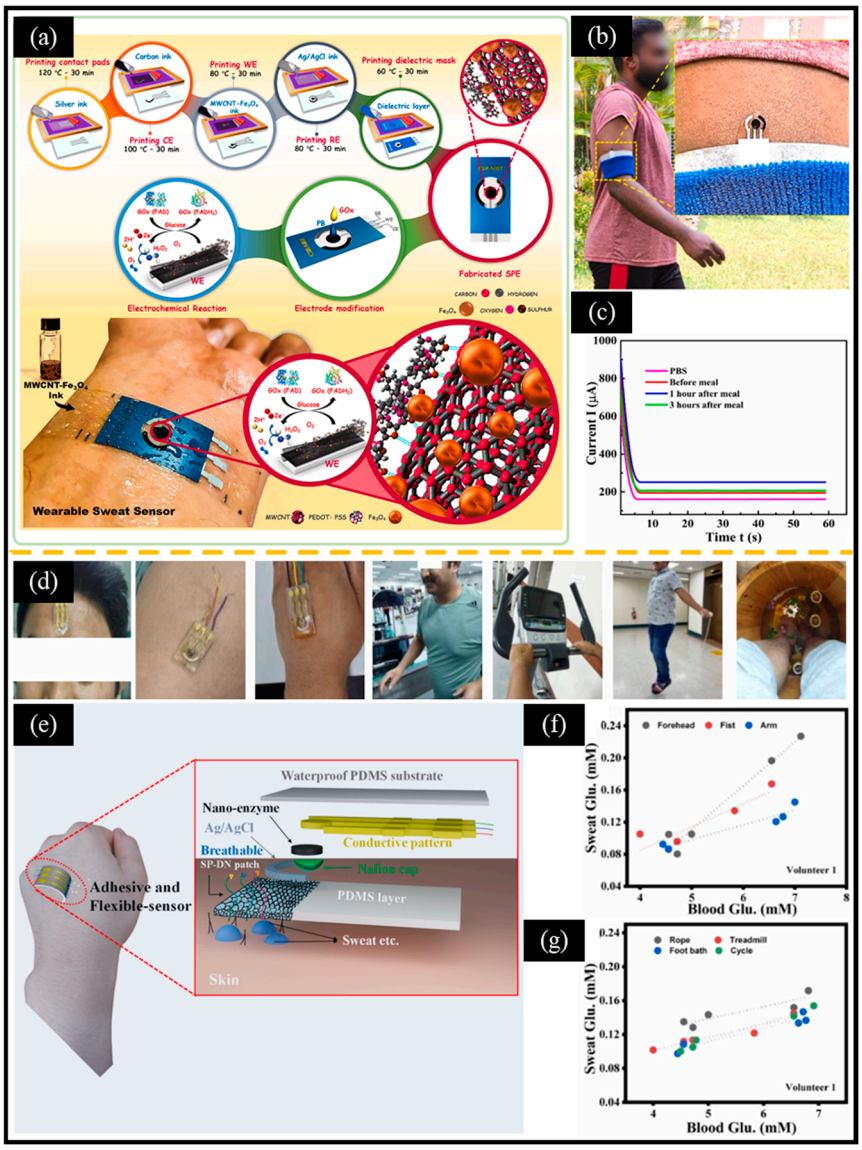

Figure 11. (**a**) Schematic diagram of printed electrodes fabricated using screen-printing technology, showing the electrochemical reaction in the presence of glucose, and a wearable sweat sensor attached to human skin. (**b**) A photo of the sensor attached to the arm while running, with an inset showing a magnified image of the sensor. (**c**) CA curves obtained from PBS and sweat samples at three different times. (**d**) Images of different sweat production methods (treadmill, cycle ergometer, skipping, and food bath). (**e**) Schematic diagram of flexible wearable sensor based on a $Co_{1.22x}Ni_xO_4$/fMWCNT nanozyme. Relationship between the blood glucose concentration and sweat glucose concentration of volunteers measured at (**f**) different sweat collection positions and under (**g**) different sweat production methods. (**a**–**c**) Reproduced with permission [153]. Copyright 2024, Elsevier. (**d**–**g**) Reproduced with permission [154]. Copyright 2024, Elsevier.

Author Contributions: Investigation, writing—original draft preparation, and writing—review and editing: H.Z.; writing—review and editing: F.S.; investigation: M.P., Y.Z., S.L. and R.L.; supervision and writing—review and editing: J.L. and Z.Y. All authors have read and agreed to the published version of the manuscript.

Funding: This work was financially supported by the National Natural Science Foundation of China (22474124, 82172345 and 81573220), the National Natural Science Foundation of Jiangsu Province (BK20221370, BK20221281), the Key University Natural Science Foundation of Jiangsu-Province (20KJA150004), the Project for Science and Technology of Yangzhou (YZ2022074), the Project for Yangzhou City and Yangzhou University corporation (YZ2023204), the Cross cooperation

project of Subei Peoples' Hospital of Jiangsu Province (SBJC22003), the Open Research Fund of State Key Laboratory of Analytical Chemistry for Life Science (no. SKLACLS2405), and the Project for Postgraduate Research & Practice Innovation Program of Jiangsu Province (no. KYCX24-3728).

Institutional Review Board Statement: Not applicable.

Informed Consent Statement: Not applicable.

Data Availability Statement: Not applicable.

Conflicts of Interest: The authors declare no conflicts of interest.

References

1. Hwang, D.W.; Lee, S.; Seo, M.; Chung, T.D. Recent advances in electrochemical non-enzymatic glucose sensors-A review. *Anal. Chim. Acta* **2018**, *1033*, 1–34. [CrossRef] [PubMed]
2. Du, Y.T.; Zhang, X.Y.; Liu, P.; Yu, D.G.; Ge, R.L. Electrospun nanofiber-based glucose sensors for glucose detection. *Front. Chem.* **2022**, *10*, 944428. [CrossRef]
3. Senjam, S.S. Diabetes and diabetic retinopathy: The growing public health concerns in India. *Lancet Global Health* **2024**, *12*, e727–e728. [CrossRef] [PubMed]
4. Shi, F.; Xu, J.M.; Hu, Z.F.; Ren, C.L.; Xue, Y.D.; Zhang, Y.C.; Li, J.; Wang, C.Y.; Yang, Z.J. Bird nest-like zinc oxide nanostructures for sensitive electrochemical glucose biosensor. *Chin. Chem. Lett.* **2021**, *32*, 3185–3188. [CrossRef]
5. Shu, Y.; Shang, Z.J.; Su, T.; Zhang, S.H.; Lu, Q.; Xu, Q.; Hu, X.Y. A highly flexible Ni-Co MOF nanosheet coated Au/PDMS film based wearable electrochemical sensor for continuous human sweat glucose monitoring. *Analyst* **2022**, *147*, 1440. [CrossRef]
6. Cho, N.H.; Shaw, J.E.; Karuranga, S.; Huang, Y.; da Rocha Fernandes, J.D.; Ohlrogge, A.W.; Malanda, B. IDF Diabetes Atlas: Global estimates of diabetes prevalence for 2017 and projections for 2045. *Diabetes Res. Clin. Pract.* **2018**, *138*, 271–281. [CrossRef]
7. Wang, J. Electrochemical glucose biosensors. *Chem. Rev.* **2008**, *108*, 814–825. [CrossRef]
8. Kiang, S.W.; Kuan, J.W.; Kuan, S.S.; Guilbault, G.G. An immobilized hexokinase enzyme stirrer for a simple and economical assay of plasma glucose. *Clin. Chim. Acta* **1977**, *78*, 495–498. [CrossRef]
9. Pham, K.; Rieta, R.; Zikos, T.; Bowen, R.; Park, W. Su1350 Analytical performance of a routinely utilized serum/plasma spectrophotometric method for glucose quantification in pancreatic cyst fluid. *Gastroenterology* **2016**, *160*, S500. [CrossRef]
10. Hoshino, T.; Takahashi, Y.; Suzuki, M. Application of high-performance liquid chromatography in establishing an accurate index of blood glucose control. *J. Chromatogr. A* **1990**, *515*, 531–536. [CrossRef]
11. Liu, Y.; Lv, R.; Sun, S.Y.; Tan, D.Y.; Dong, F.Q.; Golubev, Y.A.; Nie, X.Q.; Kotova, O.B.; Liu, J.; Wang, K. High-performance cascade nanoreactor based on halloysite nanotubes-integrated enzyme-nanozyme microsystem. *Chin. Chem. Lett.* **2022**, *33*, 807–811. [CrossRef]
12. Zhang, Q.; Li, P.P.; Wu, J.; Peng, Y.; Pang, H. Pyridine-regulated lamellar nickel-based metal-organic framework (Ni-MOF) for nonenzymatic electrochemical glucose sensor. *Adv. Sci.* **2023**, *10*, 2304102. [CrossRef] [PubMed]
13. Tong, P.H.; Wang, J.J.; Hu, X.L.; James, T.D.; He, X.P. Metal-organic framework (MOF) hybridized gold nanoparticles as a bifunctional nanozyme for glucose sensing. *Chem. Sci.* **2023**, *14*, 7762–7769. [CrossRef] [PubMed]
14. Fang, W.; Ding, L.Y.; Zhang, Y.M.; Li, H.J. Prism SPR glucose sensor based on gold nanoparticle/gold film coupling enhanced SPR. *IEEE Sens. J.* **2023**, *23*, 12477–12484. [CrossRef]
15. Zhang, X.H.; Sun, B.; Zhang, Y.Y.; Zhang, Q.F.; Akhtar, M.H.; Li, M.; Gu, Y.W.; Yu, C. Portable smartphone-assisted ratiometric fluorescence sensor for visual detection of glucose. *Anal. Chim. Acta* **2023**, *1260*, 341173. [CrossRef]
16. Saha, T.; Caño, R.D.; Mahato, K.; De la Paz, E.; Chen, C.R.; Ding, S.C.; Yin, L.; Wang, J. Wearable electrochemical glucose sensors in diabetes management: A comprehensive review. *Chem. Rev.* **2023**, *123*, 7854–7889. [CrossRef]
17. Teymourian, H.; Barfidokht, A.; Wang, J. Electrochemical glucose sensors in diabetes management: An updated review (2010–2020). Chem. *Soc. Rev.* **2020**, *49*, 7671–7709. [CrossRef]
18. Gao, Y.K.; Zhang, C.M.; Yang, Y.X.; Yang, N.; Lu, S.C.; You, T.T.; Yin, P.G. A high sensitive glucose sensor based on Ag nanodendrites/Cu mesh substrate via surface-enhanced Raman spectroscopy and electrochemical analysis. *J. Alloys Compd.* **2021**, *863*, 158758. [CrossRef]
19. He, C.H.; Asif, M.; Liu, Q.Q.; Xiao, F.; Liu, H.F.; Xia, B.Y. Noble metal construction for electrochemical nonenzymatic glucose detection. *Adv. Mater. Technol.* **2023**, *8*, 2200272. [CrossRef]
20. Xia, Y.P.; Shi, F.; Liu, R.X.; Zhu, H.B.; Liu, K.; Ren, C.L.; Li, J.; Yang, Z.J. In situ electrospinning MOF-derived highly dispersed α-cobalt confined in nitrogen-doped carbon nanofibers nanozyme for biomolecule monitoring. *Anal. Chem.* **2024**, *96*, 1345–1353. [CrossRef]
21. Zeng, J.Y.; Yang, Y.T.; Lei, X.Y.; Deng, J.A.; Hu, N.; Yang, J. Tuning Co/Ni ratio in Co-Ni bimetallic hybrid for electrochemical detection of glucose. *Chemosensors* **2024**, *12*, 38. [CrossRef]

22. Singh, K.; Maurya, K.K.; Malviya, M. Review of electrochemical sensors and biosensors based on first-row transition metals, their oxides, and noble metals nanoparticles. *J. Anal. Test.* **2024**, *8*, 143–159. [CrossRef]
23. Li, N.; Li, Q.; Yuan, M.J.; Guo, X.T.; Zheng, S.S.; Pang, H. Synthesis of $Co_{0.5}Mn_{0.1}Ni_{0.4}C_2O_4{\cdot}nH_2O$ micropolyhedrons: Multi-metal synergy for high-performance glucose catalysis. *Chem. Asian J.* **2019**, *14*, 2259–2265. [CrossRef] [PubMed]
24. Yang, Z.Y.; Bai, X.; Zhu, S.Y.; Qi, C.C. Synthesis of porous Co_3S_4 for enhanced voltammetric nonenzymatic determination of glucose. *Microchim. Acta* **2020**, *187*, 98. [CrossRef]
25. Bano, M.; Naikoo, G.A.; BaOmar, F.; Rather, J.A.; Hassan, I.U.; Sheikh, R.A.; Kannan, P.; Tambuwala, M.M. Revolutionizing glucose monitoring: Enzyme-free 2D-MoS_2 nanostructures for ultra-sensitive glucose sensors with real-time health-monitoring capabilities. *ACS Omega* **2024**, *9*, 20021–20029. [CrossRef]
26. Xia, Y.Y.; Su, T.; Mi, Z.Y.; Feng, Z.Y.; Hong, Y.W.; Hu, X.Y.; Shu, Y. Wearable electrochemical sensor based on bimetallic MOF coated CNT/PDMS film electrode via a dual-stamping method for real-time sweat glucose analysis. *Anal. Chim. Acta* **2023**, *1278*, 341754. [CrossRef]
27. Ramu, J.; Ramasundaram, S.; Yellappa, S.; Gunamalai, L.; Kamilya, T.; Afzal, M.; Jeffery, A.A.; Oh, T.H.; Mahanthappa, M.; Vishwanath, R.S. Carbon-supported nickel/nickel oxide nanohybrid composite as a high-performance sensor for electrochemical non-enzymatic glucose detection. *New J. Chem.* **2024**, *48*, 13814–13824. [CrossRef]
28. Huu Do, H.; Kim, S.Y.; Le, Q.V. Development of non-precious metal oxide-based electrodes for enzyme-free glucose detection: A review. *Microchem. J.* **2023**, *193*, 109202. [CrossRef]
29. Franceschini, F.; Payo, M.R.; Schouteden, K.; Ustarroz, J.; Locquet, J.P.; Taurino, I. MBE grown vanadium oxide thin films for enhanced non-enzymatic glucose sensing. *Adv. Funct. Mater.* **2023**, *33*, 2304037. [CrossRef]
30. Sun, F.C.; Wang, X.Z.; You, Z.H.; Xia, H.H.; Wang, S.T.; Jia, C.P.; Zhou, Y.; Zhang, J. Sandwich structure confined gold as highly sensitive and stable electrochemical non-enzymatic glucose sensor with low oxidation potential. *J. Mater. Sci. Technol.* **2022**, *123*, 113–122. [CrossRef]
31. Hilal, M.; Xie, W.F.; Yang, W. Straw-sheaf-like Co_3O_4 for preparation of an electrochemical non-enzymatic glucose sensor. *Microchim. Acta* **2022**, *189*, 364. [CrossRef] [PubMed]
32. Yang, K.; Cheng, S.S.; Yao, Z.Q.; Li, S.J.; Yang, Y.T. Dumbbell shaped nanocomposite Co_3O_4/CeO_2 derived from metal-organic frameworks (MOFs) as an excellent non-enzymatic glucose sensor. *Solid State Sci.* **2024**, *150*, 107498. [CrossRef]
33. Yuan, M.J.; Guo, X.T.; Pang, H. Derivatives (Cu/CuO, Cu/Cu_2O, and CuS) of Cu superstructures reduced by biomass reductants. *Mater. Today Chem.* **2021**, *21*, 100519. [CrossRef]
34. Gu, J.W.; Xu, Y.X.; Li, Q.; Pang, H. Porous Ni/NiO nanohybrids for electrochemical catalytic glucose oxidation. *Chin. Chem. Lett.* **2021**, *32*, 2017–2020. [CrossRef]
35. Zhou, Y.J.; Wei, W.; Lei, W.L.; Li, F.D.; Shu, J.X.; Deng, Z.X.; Hui, W.Y.; Zhao, Y.M.; Shan, C.S. Synergistically enhancing electrocatalysis and non-enzymatic sensing for glucose by iridium single-atom/nickel oxide/N-doped graphene. *Anal. Bioanal. Chem.* **2024**, *416*, 6011–6019. [CrossRef]
36. Mahar, I.A.; Tahira, A.; Parveen, M.; Hulio, A.A.; Ibupoto, Z.A.; Bhatti, M.A.; Dawi, E.; Nafady, A.; Alshammari, R.H.; Vigolo, B.; et al. Glucose sensing via green synthesis of NiO-SiO_2 composites with citrus lemon peel extract. *J. Mater. Sci. Mater. Electron.* **2024**, *35*, 490. [CrossRef]
37. Liu, Y.H.; Young, S.J.; Hsien, C.Y.; Chu, Y.L.; Wang, Z.H.; Chang, S.J. Improved non-enzymatic glucose sensors of ZnO nanorods by adsorb Pt nanoparticles. *IEEE Trans. Nanotechnol.* **2024**, *23*, 303–310. [CrossRef]
38. Sharma, S.; Ganeshan, S.K.; Kundu, S.; Chappanda, K.N. Effect of doping on TiO_2 nanotubes based electrochemical sensors: Glucose sensing as a case study. *IEEE Trans. Nanotechnol.* **2021**, *20*, 185–193. [CrossRef]
39. Zhu, J.L.; Peng, X.; Nie, W.; Wang, Y.J.; Gao, J.W.; Wen, W.; Selvaraj, J.N.; Zhang, X.H.; Wang, S.F. Hollow copper sulfide nanocubes as multifunctional nanozymes for colorimetric detection of dopamine and electrochemical detection of glucose. *Biosens. Bioelectron.* **2019**, *141*, 111450. [CrossRef]
40. Medhi, A.; Giri, M.K.; Mohanta, D. Non-enzymatic approach of H_2O_2 and glucose sensing using NiO-MoS_2-derived electrochemical sensor. *Bull. Mater. Sci.* **2024**, *47*, 223. [CrossRef]
41. Sharma, K.P.; Shin, M.; Awasthi, G.P.; Yu, C. One-pot hydrothermal synthesis of CuS/CoS composite for electrochemical non-enzymatic glucose sensor. *Curr. Appl. Phys.* **2023**, *56*, 126–134. [CrossRef]
42. Arivazhagan, M.; Santhosh, Y.M.; Maduraiveeran, G. Non-enzymatic glucose detection based on NiS nanoclusters@NiS nanosphere in human serum and urine. *Micromachines* **2021**, *12*, 403. [CrossRef] [PubMed]
43. Ghaffarirad, M.A.; Sabahi, A.; Golshani, Z.; Manteghi, F.; Ghaffarinejad, A. Non-enzymatic glucose electrochemical sensor based on nitrogen-doped graphene modified with polyaniline and Fe_3O_4@MIL-101-NH_2 nano framework. Inorg. *Chem. Commun.* **2024**, *159*, 111812. [CrossRef]
44. Ouyang, Y.C.; Zheng, X.R.; Li, Q.X.; Ye, N.B.; Mo, G.Q. ZIFs derived polyhedron with cobalt oxide nanoparticles as novel nanozyme for the biomimetic catalytic oxidation of glucose and non-enzymatic sensor. *Anal. Chim. Acta* **2022**, *1209*, 339839. [CrossRef]

45. Awais, A.; Arsalan, M.; Qiao, X.J.; Wang, Y.H.; Sheng, Q.L.; Yue, T.L.; He, Y.P. Facial synthesis of highly efficient non-enzymatic glucose sensor based on vertically aligned Au-ZnO NRs. *J. Electroanal. Chem.* **2021**, *895*, 115424. [CrossRef]
46. Chiu, W.T.; Chang, T.F.M.; Sone, M.; Mita, A.T.; Toshiyoshi, H. Electrocatalytic activity enhancement of Au NPs-TiO_2 electrode via a facile redistribution process towards the non-enzymatic glucose sensors. *Sens. Actuat. B Chem.* **2020**, *319*, 128279. [CrossRef]
47. Okamoto, K.; Kawakami, H.; Chien, Y.A.; Kurioka, T.; Chiu, W.T.; Chakraborty, P.; Nakamoto, T.; Hsu, Y.J.; Sone, M.; Chang, T.F.M. Gold/MnO_2 particles decorated on electrodeposited polyaniline toward non-enzymatic electrochemical sensor for glucose. *Micro Nano Eng.* **2023**, *18*, 100175. [CrossRef]
48. He, L.; Ma, C.Y.; Lv, G.; Liu, J.; Li, R.Z. Study on the preparation of vine-like CuS nanowires for non-enzymatic glucose sensing application. *Mater. Lett.* **2024**, *361*, 136029. [CrossRef]
49. Cao, L.H.; Yu, H.; Deng, B.H.; Li, Z.H.; Ma, L. MoS_x nanosheets supported hollow Cu_9S_5/C for electrochemical detection of glucose in human serum and beverages. *Microchem. J.* **2024**, *205*, 111238. [CrossRef]
50. Ramesh, S.; Ahmed, A.T.A.; Haldorai, Y.; Kakani, V.; Bathula, C.; Kim, H.S. Cobalt sulfide@cobalt-metal organic frame works materials for energy storage and electrochemical glucose detection sensor application. *J. Alloys Compd.* **2023**, *967*, 171760. [CrossRef]
51. Li, G.F.; Xie, G.Q.; Chen, D.; Gong, C.; Chen, X.; Zhang, Q.; Pang, B.L.; Zhang, Y.C.; Li, C.J.; Hu, J.; et al. Facile synthesis of bamboo-like Ni_3S_2@NCNT as efficient and stable electrocatalysts for non-enzymatic glucose detection. *Appl. Surf. Sci.* **2022**, *585*, 152683. [CrossRef]
52. Godarzi, S.M.; Khodadadi, A.A.; Naseh, M.V.; Mortazavi, Y. Highly stable and selective non-enzymatic glucose biosensor using carbon nanotubes decorated by Fe_3O_4 nanoparticles. *J. Electrochem. Soc.* **2014**, *161*, B19–B25. [CrossRef]
53. Ghosh, A.; Ganguly, D.; Sundara, R. A new approach to in-situ uniform growth of Fe_3O_4 nanoparticles over thermally exfoliated rGO sheet for the non-enzymatic and enzymatic detection of glucose. *J. Electroanal. Chem.* **2021**, *895*, 115386. [CrossRef]
54. Xu, J.S.; Sun, Y.T.; Zhang, J. Solvothermal synthesis of Fe_3O_4 nanospheres for high-performance electrochemical non-enzymatic glucose sensor. *Sci. Rep.* **2020**, *10*, 16026. [CrossRef] [PubMed]
55. Zhou, F.; Wang, J.Y.; Tang, Y.M.; Song, X.H.; Zhou, W.R.; Li, Y.; Gao, F. Enhanced sensing performance of flexible non-enzymatic electrochemical glucose sensors using hollow Fe_3O_4 nanospheres of controllable morphologies. *Ceram. Int.* **2024**, *50*, 38009–38021. [CrossRef]
56. Hernández-Ramírez, D.; Mendoza-Huizar, L.H.; Galán-Vidal, C.A.; Aguilar-Lira, G.Y.; Álvarez-Romero, G.A. Development of a non-enzymatic glucose sensor based on Fe_2O_3 nanoparticles-carbon paste electrodes. *J. Electrochem. Soc.* **2022**, *169*, 067507. [CrossRef]
57. Luo, L.; Cui, J.W.; Wang, Y.; Wang, Y.; Zheng, H.M.; Qin, Y.Q.; Shu, X.; Yu, D.B.; Zhang, Y.; Wu, Y.C. Synthesis of NiO/Fe_2O_3 nanocomposites as substrate for the construction of electrochemical biosensors. *J. Solid State Electrochem.* **2018**, *22*, 1763–1770. [CrossRef]
58. Abrori, S.A.; Septiani, N.L.W.; Nugraha; Anshori, I.; Suyatman; Suendo, V.; Yuliarto, B. Metal-Organic-Framework FeBDC-Derived Fe_3O_4 for non-enzymatic electrochemical detection of glucose. *Sensors* **2020**, *20*, 4891. [CrossRef]
59. Liu, L.; Wang, J.X.; Wang, C.Y.; Wang, G.X. Facile synthesis of graphitic carbon nitride/nanostructured α-Fe_2O_3 composites and their excellent electrochemical performance for supercapacitor and enzyme-free glucose detection applications. *Appl. Surf. Sci.* **2016**, *390*, 303–310. [CrossRef]
60. Qin, Y.N.; Sun, Y.J.; Li, Y.J.; Li, C.J.; Wang, L.; Guo, S.J. MOF derived Co_3O_4/N-doped carbon nanotubes hybrids as efficient catalysts for sensitive detection of H_2O_2 and glucose. *Chin. Chem. Lett.* **2020**, *31*, 774–778. [CrossRef]
61. Lu, J.H.; Cheng, C.; Cao, Y.; Hou, X.H.; Li, H.J.; Yin, X.M. MOFs-derived core-shell structured $NiCo_2O_4$ NWs@Co_3O_4 NPs for non-enzymatic glucose detection. *Ceram. Int.* **2023**, *49*, 23958–23966. [CrossRef]
62. Zhang, Y.; Zhao, Y.C.; Liu, Y.Q.; Yang, Y.Q.; Liu, X. Assist of multi-walled carbon nanotubes toward metal-organic framework chamfer cube-derived rambutan-like cobalt oxide@hollow chain and its application for non-enzymatic glucose sensing. *Appl. Surf. Sci.* **2023**, *624*, 157155. [CrossRef]
63. Mohammadpour-Haratbar, A.; Mosallanejad, B.; Zare, Y.; Rhee, K.Y.; Park, S.J. Co_3O_4 nanoparticles embedded in electrospun carbon nanofibers as free-standing nanocomposite electrodes as highly sensitive enzyme-free glucose biosensors. *Rev. Adv. Mater. Sci.* **2022**, *61*, 744–755. [CrossRef]
64. Dong, Q.C.; Wang, X.D.; Willis, W.S.; Song, D.H.; Huang, Y.K.; Zhao, J.; Li, B.K.; Lei, Y. Nitrogen-doped hollow Co_3O_4 nanofibers for both solid-state pH sensing and improved non-enzymatic glucose sensing. *Electroanalysis* **2019**, *31*, 678–687. [CrossRef]
65. Xiong, L.Y.; Kim, Y.J.; Seo, W.C.; Lee, H.K.; Yang, W.C.; Xie, W.F. High-performance non-enzymatic glucose sensor based on Co_3O_4/rGO nanohybrid. *Rare Met.* **2023**, *42*, 3046–3053. [CrossRef]
66. Mustafa, A.; Alsafari, I.A.; Somaily, H.H.; Yousaf, S.; Din, M.I.; Rahman, J.; Shahid, M.; Ashraf, M.; Warsi, M.F. Fabrication, characterization of NiO-Co_3O_4/rGO based nanohybrid and application in the development of non-enzymatic glucose sensor. *Phys. B Condens.* **2023**, *648*, 414404. [CrossRef]

67. Yin, Z.H.; He, S.S.; Li, Y.W.; Dai, W.J.; Wang, H.; He, R.H.; Tang, K.; Xiao, Y.M.; Wang, S.B.; Gao, J.; et al. Self-supported carbon electrodes with a carbon membrane and Co_3O_4 nanosheets for high-performance enzymeless glucose detection and supercapacitors. *ACS Appl. Nano Mater.* **2023**, *6*, 6208–6220. [CrossRef]
68. Manoj, D.; Aziz, A.; Muhammad, N.; Wang, Z.P.; Xiao, F.; Asif, M.; Sun, Y. Integrating Co_3O_4 nanocubes on MXene anchored CFE for improved electrocatalytic activity: Freestanding flexible electrode for glucose sensing. *J. Environ. Chem. Eng.* **2022**, *10*, 108433. [CrossRef]
69. Maghsoudi, S.; Mohammadi, A. Reduced graphene oxide nanosheets decorated with cobalt oxide nanoparticles: A nonenzymatic electrochemical approach for glucose detection. *Synth. Met.* **2020**, *269*, 116543. [CrossRef]
70. Ramesh, S.; Karuppasamy, K.; Haldorai, Y.; Sivasamy, A.; Kim, H.S.; Kim, H.S. Hexagonal nanostructured cobalt oxide@nitrogen doped multiwalled carbon nanotubes/polypyyrole composite for supercapacitor and electrochemical glucose sensor. *Colloid. Surface. B* **2021**, *205*, 111840. [CrossRef]
71. Muqaddas, S.; Javed, M.; Nadeem, S.; Asghar, M.A.; Haider, A.; Ahmad, M.; Ashraf, A.R.; Nazir, A.; Iqbal, M.; Alwadai, N.; et al. Carbon nanotube fiber-based flexible microelectrode for electrochemical glucose sensors. *ACS Omega* **2023**, *8*, 2272–2280. [CrossRef] [PubMed]
72. Shao, Z.T.; Gao, Q.Y.; Sun, S.M.; Wu, L.L.; Feng, W. MOF-derived CuO/CNT for high sensitivity and fast response glucose sensing. *Sens. Actuat. B Chem.* **2024**, *398*, 134713. [CrossRef]
73. Wang, S.Z.; Zheng, M.; Zhang, X.; Zhuo, M.P.; Zhou, Q.Q.; Su, Y.; Zheng, M.; Yuan, G.T.; Wang, Z.S. Flowerlike CuO/Au nanoparticle heterostructures for nonenzymatic glucose detection. *ACS Appl. Nano Mater.* **2021**, *4*, 5808–5815. [CrossRef]
74. Xiang, D.; Zhao, L.P.; Wang, Y.; Li, X.Z.; Sun, X.; Yang, J.K.; Liu, H.; Wan, C. A highly sensitive non-enzymatic glucose electrochemical sensor electrode material of CuO nanospheres/activated carbon composites. *Russ. J. Electrochem.* **2023**, *59*, 1194–1205. [CrossRef]
75. Carinelli, S.; Salazar-Carballo, P.A.; Melián, J.E.D.; García-García, F. Porous copper oxide thin film electrodes for non-enzymatic glucose detection. *Chemosensors* **2023**, *11*, 260. [CrossRef]
76. Kuzhandaivel, H.; Paramasivam, K.; Manickam, S.; Nallathambi, K.S. Nickel-doped CuO/Cu/Cu_2O nanocomposite as an efficient electrode for electrochemical non-enzymatic glucose sensor and asymmetric supercapacitor. *J. Appl. Electrochem.* **2023**, *53*, 1869–1886. [CrossRef]
77. He, Z.Y.; Tang, X.; Zhang, Y.; Yu, H.M.; Zou, Z.R.; Huang, K.; Xue, K.; Xiong, X.L. Rapid preparation of 3D ultra-thin CuO nanosheets by dielectric barrier discharge microplasma for non-enzymatic detection of glucose. *Catal. Lett.* **2022**, *152*, 3517–3525. [CrossRef]
78. Abd-Elrahim, A.G.; Chun, A.G. Room-temperature fabrication of a heterostructure Cu_2O@CuO nanosheet electrocatalyst for non-enzymatic detection of glucose and H_2O_2. *J. Electroanal. Chem.* **2022**, *924*, 116874. [CrossRef]
79. Patil, A.S.; Patil, R.T.; Lohar, G.M.; Fulari, V.J. Facile synthesis of CuO nanostructures for non-enzymatic glucose sensor by modified SILAR method. *Appl. Phys. A* **2021**, *127*, 101. [CrossRef]
80. Wei, C.H.N.; Zou, X.; Liu, Q.M.; Li, S.X.; Kang, C.X.; Xiang, W. A highly sensitive non-enzymatic glucose sensor based on CuS nanosheets modified Cu_2O/CuO nanowire arrays. *Electrochim. Acta* **2020**, *334*, 135630. [CrossRef]
81. Gopal, T.S.; James, J.T.; Gunaseelan, B.; Ramesh, K.; Raghavan, V.; Malathi, C.J.A.; Amarnath, K.; Kumar, V.G.; Rajasekaran, S.J.; Pandiaraj, S.; et al. MXene-embedded porous carbon-based Cu_2O nanocomposites for non-enzymatic glucose sensors. *ACS Omega* **2024**, *9*, 8448–8456.
82. Fan, B.Y.; Spindler, B.D.; Zhao, W.Y.; Chan, H.; Wang, Z.; Kim, M.; Chipangura, Y.; Bühlmann, P.; Stein, A. Comparison of Copper(II) oxide nanostructures with different morphologies for nonenzymatic glucose sensing. *ACS Appl. Nano Mater.* **2023**, *6*, 1475–1486. [CrossRef]
83. Zohaa; Arif, D.; Hassan, M.; Abdullah, M.; Miran, W.; Nasir, M.A.; Batool, S.; Baig, M.A.; Liaqat, U. An electrochemical sensor based on copper oxide nanoparticles loaded on a mesoporous MCM-41 for non-enzymatic detection of glucose. *Ceram. Int.* **2024**, *50*, 12614–12620. [CrossRef]
84. Ngo, N.T.M.; Tran, T.B.Q.; Tran, M.K.; Bui, L.A.T.; Doan, V.H.T. Synthesis of Au/Cu_2O/graphene quantum dots nanocomposites and its application for glucose oxidation. *J. Chem. Sci.* **2024**, *136*, 13.
85. Yang, Z.; Yang, H.M.; Wang, W.; Zhao, H.Y.; Meng, P.R.; Xie, Y.X.; Sun, Y. A flexible electrochemical sensor for simultaneous determination of glucose (Glu) and ethanol (Eth) using ZnO and Pd nanoparticles. *J. Appl. Electrochem.* **2023**, *53*, 2013–2023. [CrossRef]
86. Weston, M.; Kuchel, R.P.; Ciftci, M.; Boyer, C.; Chandrawati, R. A polydiacetylene-based colorimetric sensor as an active use-by date indicator for milk. *J. Colloid Interface Sci.* **2020**, *572*, 31–38. [CrossRef]
87. Myndrul, V.; Coy, E.; Babayevska, N.; Zahorodna, V.; Balitskyi, V.; Baginskiy, I.; Gogotsi, O.; Bechelany, M.; Giardi, M.T.; Iatsunskyi, I. MXene nanoflakes decorating ZnO tetrapods for enhanced performance of skin-attachable stretchable enzymatic electrochemical glucose sensor. *Biosens. Bioelectron.* **2022**, *207*, 114141. [CrossRef]

88. Morais, M.; Marques, A.C.; Ferreira, S.H.; Pinheiro, T.; Pimentel, A.; Macedo, P.; Martins, R.; Fortunato, E. Visible photoluminescent zinc oxide nanorods for label-free nonenzymatic glucose detection. *ACS Appl. Nano Mater.* **2022**, *5*, 4386–4396. [CrossRef]
89. Lin, Y.; Wu, J.W.; Tan, X.C.; Huang, K.J. Electrochemiluminescence sensor based on graphdiyne quantum dots functionalized MOF-derived ZnO with self-enhancing effect for the detection of radical scavenging drugs. *Sens. Actuat. B Chem.* **2023**, *382*, 133541. [CrossRef]
90. Mai, H.H.; Janssens, E. Au nanoparticle-decorated ZnO nanorods as fluorescent non-enzymatic glucose probe. *Microchim. Acta* **2020**, *187*, 577. [CrossRef]
91. Ali, F.; Mari, R.H.; Dawi, E.; Tahira, A.; Halepoto, I.A.; Mahar, I.A.; Rind, N.A.; Nangraj, N.A.; Bhatti, M.A.; Almani, K.F.; et al. Development of highly sensitive and selective electrochemical glucose sensors based on the modification of the surface, structural, and morphological properties of ZnO using vitamin-B complexes. *J. Electrochem. Soc.* **2024**, *171*, 077501. [CrossRef]
92. Ahmed, S.; Ashraf, M.; Yousaf, S.; Alsafari, I.A.; Akhtar, M.; Shahid, M.; Somaily, H.H.; Warsi, M.F. High-performance, non-enzymatic glucose sensor based on Fe and Cu doped ZnO/rGO based nanocomposite. *Mater. Chem. Phys.* **2023**, *297*, 127335. [CrossRef]
93. Hussein, B.A.; Tsegaye, A.A.; Shifera, G.; Taddesse, A.M. A sensitive non-enzymatic electrochemical glucose sensor based on a ZnO/Co_3O_4/reduced graphene oxide nanocomposite. *Sens. Diagn.* **2023**, *2*, 347. [CrossRef]
94. Sharma, A.; Agrawal, A.; Pandey, G.; Kumar, S.; Awasthi, K.; Awasthi, A. Carbon nano-onion-decorated ZnO composite-based enzyme-less electrochemical biosensing approach for glucose. *ACS Omega* **2022**, *7*, 37748–37756. [CrossRef]
95. Young, S.J.; Liu, Y.H.; Chu, Y.L.; Huang, J.Z. Nonenzymatic glucose sensors of ZnO nanorods modified by Au nanoparticles. *IEEE Sens. J.* **2023**, *23*, 12503–12510. [CrossRef]
96. Golli, A.E.; Echabaane, M.; Dridi, C. Development of an electrochemical nanoplatform for non-enzymatic glucose sensing based on Cu/ZnO nanocomposite. *Mater. Chem. Phys.* **2022**, *280*, 125844. [CrossRef]
97. Yao, P.; Yu, S.H.; Shen, H.F.; Yang, J.; Min, L.F.; Yang, Z.J.; Zhu, X.S. A TiO_2-SnS_2 nanocomposite as a novel matrix for the development of an enzymatic electrochemical glucose biosensor. *New J. Chem.* **2019**, *43*, 16748–16752. [CrossRef]
98. Li, M.Z.; Zhang, Y.; Li, K.; Shang, Y.N.; Zhang, Y.Z.; Kan, Y.J.; Jiao, Z.Y.; Han, Y.Y.; Cao, X.Q. In situ regeneration of catalyst for Fenton-like degradation by photogenerated electron transportation: Characterization, performance and mechanism comparison. *Chin. Chem. Lett.* **2025**, *36*, 109885. [CrossRef]
99. Yadav, M.; Lata, S.; Singh, G. Revisiting some recently developed conducting polymer@metal oxide nanostructures for electrochemical sensing of vital biomolecules: A review. *J. Anal. Test.* **2022**, *6*, 274–295. [CrossRef]
100. Lu, C.Y.; Ma, Y.Y.; Cao, Y.; Huang, Q.G.; Wang, J.L. Fluorine doping-induced oxygen vacancy-rich TiO_2 via contact activation for signal boosting in electrochemical sensing. *Chem. Eng. J.* **2023**, *468*, 143598. [CrossRef]
101. Yang, Z.; Xu, W.; Yan, B.D.; Wu, B.Q.; Ma, J.X.; Wang, X.H.; Qiao, B.; Tu, J.C.; Pei, H.; Chen, D.L.; et al. Gold and platinum nanoparticle-functionalized TiO_2 nanotubes for photoelectrochemical glucose sensing. *ACS Omega* **2022**, *7*, 2474–2483. [CrossRef] [PubMed]
102. Shen, B.; Wu, Q.; Fan, Y.P.; Wu, H.P.; Li, X.M.; Zhao, X.F.; Wang, Y.W.; Ding, S.J.; Zhang, J. TiO_2@Ag nanozyme enhanced electrochemiluminescent biosensor coupled with DNA nanoframework-carried emitters and enzyme-assisted target recycling amplification for ultrasensitive detection of microRNA. *Chem. Eng. J.* **2022**, *445*, 136820. [CrossRef]
103. Caglar, A.; Aktas, N.; Kivrak, H. Tailoring cadmium composition on titanium dioxide to achieve enhanced photocatalytic glucose fuel cell anode performance. *ACS Appl. Energy Mater.* **2021**, *4*, 12298–12309. [CrossRef]
104. Wu, P.L.; Fan, J.W.; Tai, Y.Z.; He, X.; Zheng, D.D.; Yao, Y.C.; Sun, S.J.; Ying, B.W.; Luo, Y.; Hu, W.C.; et al. Ag@TiO_2 nanoribbon array: A high-performance sensor for electrochemical non-enzymatic glucose detection in beverage sample. *Food Chem.* **2024**, *447*, 139018. [CrossRef]
105. Kang, Y.; Ren, X.L.; Li, Y.J.; Yu, Z.M. Ni-coated diamond-like carbon-modified TiO_2 nanotube composite electrode for electrocatalytic glucose oxidation. *Molecules* **2022**, *27*, 5815. [CrossRef]
106. Jeong, H.; Yoo, J.; Park, S.; Lu, J.L.; Park, S.; Lee, J. Non-enzymatic glucose biosensor based on highly pure TiO_2 nanoparticles. *Biosensors* **2021**, *11*, 149. [CrossRef]
107. Kumar, B.; Sinha, S.K. Nanostructured Cu_2O deposited on TiO_2 nanotube arrays for ultra-sensitive non-enzymatic glucose electrochemical biosensor. *Ionics* **2023**, *29*, 793–805. [CrossRef]
108. Chen, L.J.; Gao, H.Y.; Bai, Y.; Wei, W.; Wang, J.F.; Fakhri, G.E.; Wang, M.Y. Colorimetric biosensing of glucose in human serum based on the intrinsic oxidase activity of hollow MnO_2 nanoparticles. *New J. Chem.* **2020**, *44*, 15066–15070. [CrossRef]
109. Seifi, A.; Afkhami, A.; Madrakian, T. Improved MnO_2 based electrode performance arising from step by step heat treatment during electrodeposition of MnO_2 for determination of paracetamol, 4-aminophenol, and 4-nitrophenol. *Sci. Rep.* **2024**, *14*, 26577. [CrossRef]
110. Gricar, E.; Radic, J.; Genorio, B.; Kolar, M. Highly sensitive and selective graphene nanoribbon based enzymatic glucose screen-printed electrochemical sensor. *Sensors* **2022**, *22*, 9590. [CrossRef]

111. Juang, F.R.; Wang, T.M. Surfactant-free synthesis of self-assembled CuO spheres composited with MnO_2 nanorods for non-enzymatic glucose detection. *Physica E Low Dimens. Syst. Nanostruct.* **2021**, *134*, 114831. [CrossRef]
112. Huang, M.; Feng, S.; Yang, C.; Wen, F.; He, D.; Jiang, P. Construction of an MnO_2 nanosheet array 3D integrated electrode for sensitive enzyme-free glucose sensing. *Anal. Methods* **2021**, *13*, 1247–1254. [CrossRef] [PubMed]
113. Jadhav, S.B.; Malavekar, D.B.; Kale, S.B.; Sabale, S.R.; Patil, U.M.; Lokhande, C.D.; Pawaskar, P.N. Reliable glucose sensing properties of electrodeposited vertically aligned manganese oxide thin flm electrode. *Appl. Phys. A* **2021**, *127*, 391. [CrossRef]
114. Yin, Z.Y.; Allado, K.; Sheardy, A.T.; Ji, Z.W.; Arvapalli, D.; Liu, M.X.; He, P.; Zeng, X.P.; Wei, J.J. Mingled MnO_2 and Co_3O_4 binary nanostructures on well-aligned electrospun carbon nanofibers for nonenzymatic glucose oxidation and sensing. *Cryst. Growth Des.* **2021**, *21*, 1527–1539. [CrossRef]
115. Wang, S.; Zhang, D.; Li, B.; Zhang, C.; Du, Z.G.; Yin, H.M.; Bi, X.F.; Yang, S.B. Ultrastable in-plane 1T-2H MoS_2 heterostructures for enhanced hydrogen evolution reaction. *Adv. Energy Mater.* **2018**, *8*, 1801345. [CrossRef]
116. Li, X.; Li, Q.; Yan, W.J.; Fan, B.B.; Wang, Z.D. In-situ controllable electrodeposition of NiS_x nanostructures coupled with polypyrrole for enhanced hydrogen evolution reaction. *Int. J. Hydrogen Energy* **2024**, *51*, 443–451. [CrossRef]
117. Liu, Y.; Jin, H.J.; Zou, W.T.; Guo, R. Protein-mediated sponge-like copper sulfide as an ingenious and efficient peroxidase mimic for colorimetric glucose sensing. *RSC Adv.* **2020**, *10*, 28819–28826. [CrossRef]
118. Zhang, Y.; Gao, Y.M.; Zhang, S.; Huang, Y.Y.; Wei, Y.; Cai, H.S.; Jia, Z.F.; Su, X.D. Au-wrapped CuS-interlaced chain structure for ultrafast response and high sensitive non-enzymatic glucose sensor. *J. Electrochem. Soc.* **2023**, *170*, 057509. [CrossRef]
119. Zhou, X.; Ling, S.Q.; Lin, Z.H.; Wu, Y.X.; Bao, J.; Liu, X. Low-applied potential non-enzymatic glucose sensor based on ultrathin 2-D CuS nanowall arrays. *Electroanalysis* **2021**, *33*, 2204–2215. [CrossRef]
120. Cao, W.B.; Guo, T.; Ding, Y.G.; Hu, Y.M.; Liu, D. Substantially boosting the performance of non-enzymatic glucose sensing: Introducing a novel CuS nanosheet anchored on hollow $Ni(OH)_2$ nanosphere. *Appl. Surf. Sci.* **2023**, *634*, 157650. [CrossRef]
121. Yang, T.; Zhang, W.N.; Wu, J.S.; Liu, S.; Zhao, Y. Core-shell composite of CuS nanocages and NiCo layered double hydroxide nanosheets with modulated electron structure as "two birds with one Stone" glucose oxidation electrocatalysts. *Appl. Surf. Sci.* **2022**, *600*, 154205. [CrossRef]
122. Choi, M.; Lee, G.; Lee, Y.L.; Lee, H.; Yang, J.H.; Jang, H.; Han, H.; Kang, M.S.; Yoo, S.; Jang, A.R.; et al. Transferable, highly crystalline covellite membrane for multifunctional thermoelectric systems. *InfoMat* **2024**, *6*, e12626. [CrossRef]
123. Cho, D.; Lee, G.; Lee, Y.L.; Cho, A.; Lee, S.; Kim, G.H.; Park, G.; Jang, S.; Choi, M.; Shim, Y.S.; et al. Ultrathin copper monosulfide films for an optically semitransparent, highly selective ammonia chemosensor. *ACS Appl. Mater. Interfaces* **2024**, *16*, 60530. [CrossRef]
124. Mai, L.N.T.; Tran, T.H.; Bui, Q.B.; Nhac-Vu, H.T. A novel nanohybrid of gold nanoparticles anchored copper sulfide nanosheets as sensitive sensor for nonenzymatic glucose detection. *Colloid. Surface. A* **2019**, *582*, 123936. [CrossRef]
125. Sharma, K.P.; Shin, M.; Awasthi, G.P.; Poudel, M.B.; Kim, H.J.; Yu, C. Chitosan polymer matrix-derived nanocomposite (CuS/NSC) for non-enzymatic electrochemical glucose sensor. *Int. J. Biol. Macromol.* **2022**, *206*, 708–717. [CrossRef]
126. Abidi, I.H.; Giridhar, S.P.; Tollerud, J.O.; Limb, J.; Waqar, M.; Mazumder, A.; Mayes, E.L.H.; Murdoch, B.J.; Xu, C.; Bhoriya, A.; et al. Oxygen driven defect engineering of monolayer MoS_2 for tunable electronic, optoelectronic, and electrochemical devices. *Adv. Funct. Mater.* **2024**, *34*, 2402402. [CrossRef]
127. Hu, Z.F.; Xu, R.; Yu, S.H.; Li, J.; Yang, Z.J. Facile synthesis of a nanorod-like MoS_2 nanostructure for sensitive electrochemical biosensing application. *Analyst* **2020**, *145*, 7864–7869. [CrossRef]
128. Huang, T.X.; Cong, X.; Wu, S.S.; Wu, J.B.; Bao, Y.F.; Cao, M.F.; Wu, L.W.; Lin, M.L.; Tan, P.H.; Ren, B. Visualizing the structural evolution of individual active sites in MoS_2 during electrocatalytic hydrogen evolution reaction. *Nat. Catal.* **2024**, *7*, 646–654. [CrossRef]
129. Kumar, B.A.; Ramalingam, G.; Al Omari, S.A.B.; Bakenov, Z.; Sangaraju, S.; Sudhakar, S. Efficient processed carbon Soot@MoS_2 hybrid Bi-functional electrode for dye-sensitized solar cell and asymmetric supercapacitor devices. *Nano Mater. Sci.* **2024**, *6*, 484–494. [CrossRef]
130. Sharma, K.P.; Shin, M.; Awasthi, G.P.; Cho, S.; Yu, C. One-step hydrothermal synthesis of CuS/MoS_2 composite for use as an electrochemical non-enzymatic glucose sensor. *Heliyon* **2024**, *10*, e23721. [CrossRef]
131. Luo, Y.Y.; Xiang, Y.J.; Qin, L.R.; Zhao, J.W.; He, H.M.; Liu, Y.X. Screen-printed electrode modified with MoO_3-MoS_2/Ni porous array for sensitive non-enzymatic glucose sensor. *Sensor. Actuat. A Phys.* **2023**, *364*, 114817. [CrossRef]
132. Li, J.; Liu, Y.T.; Tang, X.; Xu, L.J.; Min, L.F.; Xue, Y.D.; Hu, X.Y.; Yang, Z.J. Multiwalled carbon nanotubes coated with cobalt(II) sulfide nanoparticles for electrochemical sensing of glucose via direct electron transfer to glucose oxidase. *Microchim. Acta* **2020**, *187*, 80. [CrossRef]
133. Naderi, L.; Shahrokhian, S.; Amini, M.K.; Kahnamouei, M.H. Comparison of electrocatalytic performance of $CuCo_2O_4$ nanorods and nanospheres decorated with Co_3S_4 nanosheets for electrochemical sensing of hydrogen peroxide and glucose in human serum. *ACS Appl. Nano Mater.* **2023**, *6*, 2755–2769. [CrossRef]

134. Sridhar, V.; Park, H. Carbon encapsulated cobalt sulfide nano-particles anchored on reduced graphene oxide as high capacity anodes for sodium-ion batteries and glucose sensor. *J. Alloys Compd.* **2018**, *764*, 490–497. [CrossRef]
135. Qi, Y.L.; Hu, Y.A.; Wu, X.C.; Wu, W.X.; Bao, J.; Yang, H.S.; Zhao, J.Y.; Hou, C.J.; Huo, D.Q. Self-supporting flexible enzyme-free sensor based on CoS-PPy-CP for glucose detection. *J. Electrochem. Soc.* **2021**, *168*, 107507. [CrossRef]
136. Gharani, M.; Bahari, A.; Ghasemi, S. MOF-derived MoS_2@Co_3S_4 nanoparticles modified with Ag as efficient sensor for glucose determination. *Synth. Met.* **2023**, *293*, 117252. [CrossRef]
137. Tan, Z.; Huang, Y.L.; Wang, S.Q.; Feng, C.Q.; Sun, Z.G.; Wu, H.M.; Zhang, Y.Q. Production of Ni_7S_6/NiO hybrids as a highly sensitive amperometric sensor for glucose. *Ionics* **2019**, *25*, 3961–3969. [CrossRef]
138. Kuznowicz, M.; Rebis, T.; Jedrzak, A.; Nowaczyk, G.; Jesionowski, T. Facile fabrication of a selective poly(caffeic acid)@MWCNT-$Ni(OH)_2$ hybrid nanomaterial and its application as a non-enzymatic glucose sensor. *Chemosensors* **2023**, *11*, 452. [CrossRef]
139. Ensafi, A.A.; Mirzaii, F.; Nasr-Esfahani, P.; Rezaei, B. Ni_3S_2 supported on porous ball-milled silicon, a highly selective electrochemical sensor for glucose determination. *Electroanal.* **2020**, *32*, 1707–1716. [CrossRef]
140. El-Wekil, M.M.; Hayallah, A.M.; Abdelgawad, M.A.; Abourehab, M.A.S.; Shahin, R.Y. Nanocomposite of gold nanoparticles@nickel disulfide-plant derived carbon for molecularly imprinted electrochemical determination of favipiravir. *J. Electroanal. Chem.* **2022**, *922*, 116745. [CrossRef]
141. Arivazhagan, M.; Maduraiveeran, G. Ultra-fine nickel sulfide nanoclusters@nickel sulfide microsphere as enzyme-free electrode materials for sensitive detection of lactic acid. *J. Electroanal. Chem.* **2020**, *874*, 114465. [CrossRef]
142. Sunil Kumar Naik, T.S.; Saravanan, S.; Sri Saravana, K.N.; Pratiush, U.; Ramamurthy, P.C. A non-enzymatic urea sensor based on the nickel sulfide/graphene oxide modified glassy carbon electrode. *Mater. Chem. Phys.* **2020**, *245*, 122798. [CrossRef]
143. Kannan, P.; Chen, F.S.; Jiang, H.S.; Wang, H.; Wang, R.F.; Subramanian, P.; Ji, S. Hierarchical core-shell structured Ni_3S_2/$NiMoO_4$ nanowires: A high-performance and reusable electrochemical sensor for glucose detection. *Analyst* **2019**, *144*, 4925–4934. [CrossRef]
144. Kim, S.; Lee, S.H.; Cho, M.; Lee, Y. Solvent-assisted morphology confinement of a nickel sulfide nanostructure and its application for non-enzymatic glucose sensor. *Biosens. Bioelectron.* **2016**, *85*, 587–595. [CrossRef]
145. Mazurków, J.M.; Kusior, A.; Mikuła, A.; Radecka, M. Predicting sensitivity to glucose in metal sulfides: A structural and surface characterization study. *J. Alloys Compd.* **2024**, *1004*, 175749. [CrossRef]
146. Meng, A.; Hong, X.C.; Zhang, H.Q.; Tian, W.L.; Li, Z.J.; Sheng, L.Y.; Li, Q.D. Nickel sulfide nanoworm network architecture as a binder-free high-performance non-enzymatic glucose sensor. *Microchim. Acta* **2021**, *188*, 34. [CrossRef]
147. Qian, X.; Ko, A.; Li, H.F.; Liao, C.Z. Flexible non-enzymatic glucose strip for direct non-invasive diabetic management. *Microchem. J.* **2024**, *197*, 109818. [CrossRef]
148. Osuna, V.; Martínez, E.P.A.; Dominguez, R.B.; Rios, A.V. A Review on the advances in nanomaterials for electrochemical non-enzymatic glucose sensors working in physiological conditions. *Chemosensors* **2024**, *12*, 159. [CrossRef]
149. Benedetti, T.M.; Somerville, S.V.; Wordsworth, J.; Yamamoto, Y.; Schuhmann, W.; Tilley, R.D.; Gooding, J.J. An artificial enzyme: How nanoconfinement allows the selective electrochemical detection of glucose directly in whole blood. *Adv. Funct. Mater.* **2024**, *34*, 2400322. [CrossRef]
150. Zhong, X.; He, Z.Y.; Chen, H.J.; Chen, Y. Enhancing the non-enzymatic glucose detection performance of $Ni(OH)_2$ nanosheets via defect engineering. *Surf. Interfaces* **2021**, *25*, 101234. [CrossRef]
151. Zhou, Z.Z.; Wang, L.J.; Wang, J.; Liu, C.H.; Xu, T.L.; Zhang, X.J. Machine learning with neural networks to enhance selectivity of nonenzymatic electrochemical biosensors in multianalyte mixtures. *ACS Appl. Mater. Interfaces* **2022**, *14*, 52684–52690. [CrossRef] [PubMed]
152. Zhu, J.; Liu, S.B.; Hu, Z.H.; Zhang, X.Z.; Yi, N.; Tang, K.R.; Dexheimer, M.G.; Lian, X.J.; Wang, Q.; Yang, J.; et al. Laser-induced graphene non-enzymatic glucose sensors for on body measurements. *Biosens. Bioelectron.* **2021**, *193*, 113606. [CrossRef] [PubMed]
153. Shamili, C.; Pillai, A.S.; Saisree, S.; Chandran, A.; Varma, M.R.; Peethambharan, S.K. All-printed wearable biosensor based on MWCNT-iron oxide nanocomposite ink for physiological level detection of glucose in human sweat. *Biosens. Bioelectron.* **2024**, *258*, 116358. [CrossRef] [PubMed]
154. Shrestha, D.; Kang, K.; Nayaju, T.; Bacirhonde, P.M.; Maharjan, B.; Park, C.H.; Kim, C.S. $Co_{1.22x}Ni_xO_4$/fMWCNTs-hybrid nanocomposite-based self-adhesive wearable non-enzymatic electrochemical sensor for continuous glucose monitoring in sweat. *Colloid. Surface. A* **2024**, *686*, 133361. [CrossRef]
155. Kim, C.H.; Lee, D.H.; Youn, J.; Lee, H.; Jeong, J. Simple and cost-effective microfabrication of flexible and stretchable electronics for wearable multi-functional electrophysiological monitoring. *Sci. Rep.* **2021**, *11*, 14823. [CrossRef]